Well-defined Surface Catalytic Sites for Solar CO_2 Reduction: Heterogenized Molecular Catalysts and Single Atom Catalysts

Peipei Huang, Ehab Shaaban, Esraa Ahmad, Allison St. John, Tianqi Jin, and Gonghu Li *

Department of Chemistry, University of New Hampshire, Durham NH 03824, United States

Abstract

Exciting progress has been made in the area of solar fuel generation by CO_2 reduction. New photocatalytic materials containing well-defined surface catalytic sites have emerged in recent years, including heterogenized molecular catalysts and single atom catalysts. This Feature Article summarizes our recent research in this area, together with brief discussions of relevant literature. In our effort to obtain heterogenized molecular catalysts, a diimine-tricarbonyl Re(I) complex and a tetraaza macrocyclic Co(III) compound were covalently attached to different surfaces, and the effects of ligand derivatization and surface characteristics on their structures and photocatalytic activities were investigated. Single atom catalysts combine the advantages of homogeneous and heterogeneous catalysis. A single-site cobalt catalyst was prepared on graphitic carbon nitride, which demonstrated excellent activity in selective CO_2 reduction under visible-light irradiation. Doping carbon nitride with carbon was found to have profound effects on the structure and activity of the single-site cobalt catalyst. Our research achievements are presented to emphasize how spectroscopic techniques, including infrared, UV-visible, electron paramagnetic resonance, and X-ray absorption spectroscopies, could be combined with catalyst synthesis and computation modeling to understand the structures and properties of well-defined surface catalytic sites at the molecular level. This article also highlights challenges and opportunities in the broad context of solar CO_2 reduction.

1. Introduction

Carbon dioxide (CO_2) is considered a renewable C1 feedstock for the production of valuable chemicals and fuels.[1, 2] Sufficient energy and catalysts are needed to activate CO_2, which is a very stable molecule. Solar-driven CO_2 reduction has been extensively investigated in recent years as it employs natural sunlight as a renewable energy source. Various photocatalysts capable of activating CO_2 under light irradiation have been reported in the literature, including molecular complexes, inorganic semiconductors, and other systems.[3-7]

In molecular systems, the photocatalyst could be a transition metal complex that can harvest light and activate CO_2, or a molecular CO_2-reduction catalyst combined with a photosensitizer.[8-11] An example of the former is $Re(bpy)(CO)_3Cl$ (denoted "Re–bpy"), where bpy is 2,2′-bipyridine. This diimine-tricarbonyl Re(I) compound and its supramolecular complexes have demonstrated excellent reactivity and selectivity towards CO formation in photocatalytic CO_2 reduction.[12, 13] Examples of the latter include $[Co(cyclam)Cl_2]Cl$ (denoted "Co–cyclam"), where cyclam is 1,4,8,11-tetraazacy-clotetradecane. This macrocyclic complex requires the use of photosensitizers, such as *p*-terphenyl, to harvest light and generate electrons needed for CO_2 reduction.[14, 15] While these molecular photocatalysts are highly active and selective towards CO_2 reduction, many suffer from poor stability under photochemical conditions. In addition, most molecular complexes require the use of non-renewable electron donors to maintain reactivity in CO_2-reduction photocatalysis.

In comparison, inorganic semiconductors,[16-21] most notably titanium dioxide (TiO_2)-based materials, are robust heterogeneous photocatalysts for CO_2 reduction since the early work by Inoue and co-workers.[22] One attractive feature of such photocatalysts is that some semiconductors (e.g. TiO_2) with appropriate band positions allow the use of water as a renewable electron donor for

CO_2 reduction. However, most semiconductor photocatalysts are inefficient in converting photonic energy into chemical energy due to recombination of photogenerated charge carriers (electrons and holes) that prevails in the bulk.[23, 24] Furthermore, such heterogeneous photocatalysts often lack well-defined surface sites for selective CO_2 reduction.

Different strategies have been designed to prepare robust and efficient photocatalysts containing well-defined surface catalytic sites (Figure 1). For instance, heterogenized molecular catalysts can be obtained by attaching molecular catalysts onto light-absorbing surfaces.[25-31] Such photocatalysts generally show enhanced activity and improved photostability. Atomically dispersed catalysts or single-atom catalysts (SACs) are known to have well-defined active sites on a solid support.[32-39] SACs have demonstrated distinct properties in a wide range of chemical reactions, including photocatalysis.[40-43] Recently, there has been enormous interest in developing SACs for use in solar CO_2 reduction.[44-48]

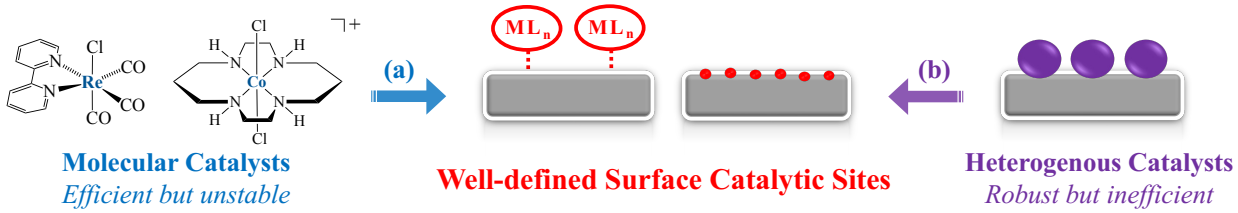

Figure 1. Approaches to obtain well-defined surface catalytic sites for efficient solar CO_2 reduction: (a) heterogenization of molecular catalysts and (b) atomic dispersion of supported metal nanoparticles. Re–bpy and Co–cyclam are shown here as examples of molecular CO_2-reduction catalysts (ML_n). The third Cl^- ligand for Co–cyclam is not shown here.

This Feature article summarizes our recent effort to construct well-defined catalytic sites on surface for use in solar CO_2 reduction. In particular, Re–bpy and Co–cyclam were attached to different surfaces to obtain heterogenized molecular catalysts. These two complexes were chosen in our studies due to their well-known activity in CO_2-reduction catalysis and their relatively

simple molecular structures that allow facile ligand derivatization for surface attachment. Our research in this direction has been focused on the effects of ligand derivatization and surface characteristics on the photocatalytic activities of the heterogenized molecular catalysts. As will be discussed, heterogenization of the molecular catalysts on surfaces allowed us to investigate their structures and complexation using spectroscopic techniques, which could be less informative and more challenging in studying the molecular catalysts in homogeneous solutions. Inspired by the CO_2-reduction activity of Co–cyclam and prior work by others in the area of SACs, we discovered a Co SAC on graphitic carbon nitride (C_3N_4) capable of catalyzing selective CO_2 reduction under visible-light irradiation. The Co SAC structure was interrogated by using a combination of synthesis, spectroscopy, and modeling studies. Relevant research results by others are also discussed to highlight the progress and challenges in the broad context of solar CO_2 reduction using innovative photocatalysts.

2. Solar CO_2 Reduction using Re–bpy Covalently Attached to SiO_2

As a model molecular catalyst, Re–bpy has been covalently attached to semiconductor surfaces,[49-57] including photoelectrodes,[58, 59] to achieve selective CO_2 reduction under solar irradiation. Despite the fact that Re–bpy itself is capable of catalyzing CO_2 reduction under light irradiation, the semiconductor support could further improve the photocatalytic performance of Re–bpy. For example, Windle and co-workers[52] prepared a diimine-tricarbonyl Re(I) complex derivatized with phosphonate groups for immobilization on a TiO_2 surface. The heterogenized Re(I) catalyst demonstrated significantly higher activity than Re–bpy in solar CO_2 reduction under the same condition. Results obtained using transient absorption spectroscopy revealed that the enhancement in activity upon heterogenization was due to an increase in the lifetime of a reduced

Re intermediate on the TiO_2 surface. A later study by Abdellah and co-workers[53] revealed the role of TiO_2 as an electron reservoir, slowing down charge recombination and improving photocatalysis.

We employ SiO_2 as a model support for Re–bpy to carry out spectroscopic investigations since (i) SiO_2 is almost "transparent" in studies using many spectroscopic techniques, and (ii) Re–bpy itself is capable of harvesting light and mediating CO_2 reduction. Our research in this area has been focused on the effects of ligand derivatization and surface water on the complexation and activity of heterogenized Re–bpy.

2.1. Covalent Attachment of Re–bpy onto SiO_2 via Amide Linkages

In our initial study, Re–bpy was physically adsorbed on a hierarchical mesoporous zeolite.[60] Diffuse reflectance infrared Fourier transform spectroscopy (DRIFTS) was employed to examine the adsorption and complexation of Re–bpy upon light irradiation. In the presence of CO_2 and an electron donor, the formation of important reaction intermediates, including Re–carboxylato and Re–formato species, was observed upon light irradiation.[60] This initial work allowed us to establish experimental protocols for investigating molecular catalysts on surfaces in the absence of organic solvents.

Covalent attachment of Re–bpy on SiO_2 was achieved via two approaches (Scheme 1), both of which involved the derivatization of bpy with chlorocarbonyl groups.[61, 62] In the first approach (Scheme 1a), a bpy-functionalized SiO_2 (denoted "L–SiO_2") was obtained in the reaction between a SiO_2 surface and a bpy-containing silane coupling agent. In the second approach (Scheme 1b), the SiO_2 surface was functionalized with an amino silane coupling agent prior to

reacting with the derivatized bpy ligand. The reaction between L–SiO_2 and $Re(CO)_5Cl$ led to the covalent attachment of Re–bpy on SiO_2 via amide linkages.

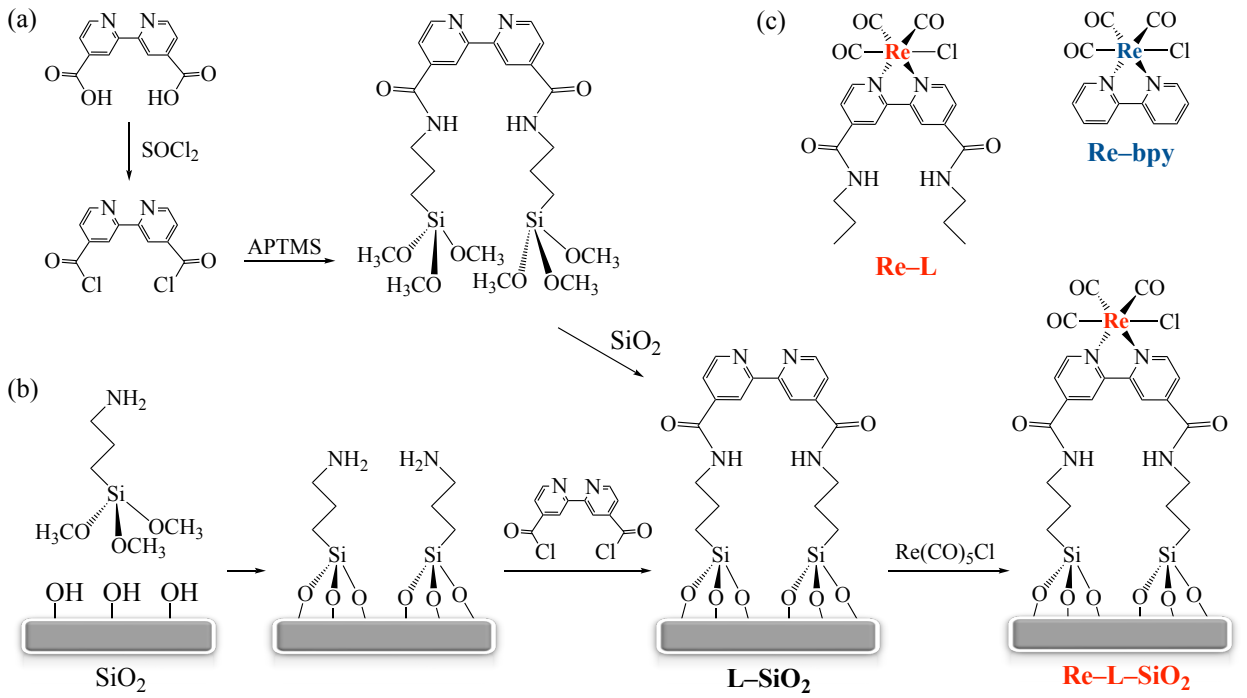

Scheme 1. Two synthetic routes for covalently attaching Re–bpy to a SiO_2 surface containing silanol groups (a and b). APTMS: 3-aminopropyltrimethoxysilane. The molecular structures of two homogeneous Re(I) complexes are shown in (c).

The heterogenized Re–bpy, denoted "Re–L–SiO_2", was characterized with DRIFTS to confirm the successful surface immobilization. Figure 2 shows the DRIFTS spectra of SiO_2, Re–bpy physically adsorbed on SiO_2, L–SiO_2, and Re–L–SiO_2. An intense absorption at 3745 cm^{-1} featuring surface silanol (Si–OH) groups is present in the spectra of SiO_2 and Re–bpy physically adsorbed on SiO_2 (Figure 2, a and b). This peak is absent in the spectrum of L–SiO_2 shown in Figure 2c since the silanol groups were consumed upon functionalizing the SiO_2 surface with the silane coupling agent. Further supporting this is the presence of infrared absorptions associated with the amide linkages at 1376 cm^{-1} (C–N stretch), 1548 cm^{-1} (N–H bend), and 1657 cm^{-1} (C=O

stretch) as well as the methylene C–H stretching bands around 2800–3000^{-1} (not labeled) shown in Figure 2c. Compared to the spectrum of L–SiO_2, the spectrum of Re–L–SiO_2 contains two additional broad absorptions at 1903 cm^{-1} and 2026 cm^{-1} characteristic of surface Re(I)–carbonyl groups (Figure 2d), indicating Re–bpy was successfully grafted on SiO_2 through amide linkages.[61]

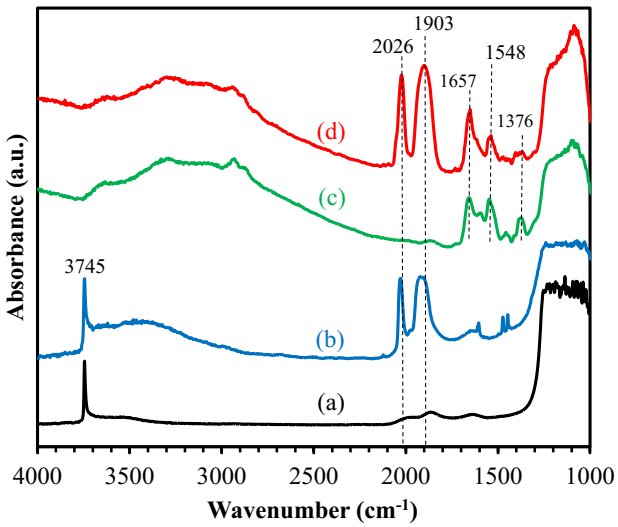

Figure 2. DRIFTS spectra of (a) SiO_2, (b) Re–bpy physically adsorbed on SiO_2, (c) L–SiO_2, and (d) Re–L–SiO_2. Adapted with permission from *J. Mol. Catal. A* 2012, 363-364, 208-213. Copyright 2012 Elsevier.

The characteristic carbonyl infrared bands have been utilized to probe the configurations of Re(I) complexes on surfaces. Anfuso and co-workers[50] shown that a Re(I) complex bearing –COOH groups was bound to TiO_2 through the carboxylate groups in bidentate or tridentate linkage motifs. The surface Re(I) complex had the bpy moiety nearly perpendicular to the TiO_2 surface, exposing the Re(I) complex to the solution in a configuration suitable for catalysis.

2.2. Effects of Derivatizing the bpy Ligand with Amide Groups

Derivatization of the bpy ligand with amide groups allowed the successful surface immobilization of Re–bpy on SiO_2. However, such ligand derivatization resulted in significantly changes in the photophysical and photochemical properties of Re–bpy. For instance, the ultraviolet-visible (UV-vis) spectrum of Re–bpy physically adsorbed on SiO_2 (Figure 3a, solid trace) features an intense absorption at 365 nm, which is associated with the metal-to-ligand charge transfer (MLCT) transition of Re–bpy on the surface.[63] In comparison, the spectrum of the heterogenized Re(I) catalyst, Re–L–SiO_2, has an MLCT band at 400 nm (Figure 3b, solid trace).

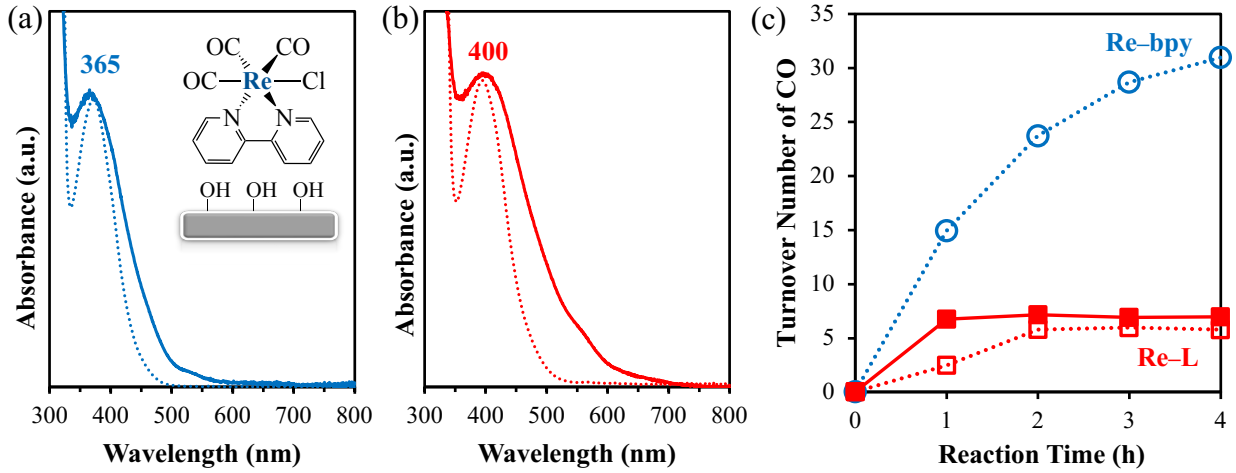

Figure 3. Diffuse reflectance UV–vis spectra of (a) Re–bpy physically adsorbed on SiO_2 and (b) Re–L–SiO_2. The UV–vis spectra of corresponding molecular complexes (Re–bpy and Re–L) in organic solvents are also shown (dotted traces). Adapted with permission from *J. Mol. Catal. A* 2012, 363-364, 208-213. Copyright 2012 Elsevier. (c) Production of CO in solar CO_2 reduction using Re–bpy (open circle), Re–L (open square) and Re–L–SiO_2 (solid square). Adapted with permission from *ACS Catal.* 2013, 3, 655-662. Copyright 2013 American Chemical Society.

In order to explore the origin of this observed red shift, a homogeneous compound, Re–L (see Scheme 1c for its structure), was synthesized by derivatizing Re–bpy with amide groups. The MLCT transition of the homogeneous Re–L occurs around 395 nm in contrast with 371 nm for Re–bpy (Figure 3, a and b, dotted traces). Therefore, the red shift observed in Figure 3 (a and b) originated from the ligand derivatization. It is noteworthy that the MLCT bands of surface Re(I)

complexes (Figure 3, a and b, solid traces) are much broader than those of the corresponding homogeneous complexes (Figure 3, a and b, dotted traces). This peak broadening is a strong indication of heterogeneity of the surface Re(I) complexes.

We further revealed that the ligand derivatization significantly altered the electrochemical and photocatalytic properties of Re–bpy.[62] The presence of electron–withdrawing amide groups in Re–L shifted the redox potentials of Re–bpy to more positive values. Consequently, the activity of Re–L was found to be much lower than Re–bpy in photocatalytic CO_2 reduction under simulated solar irradiation (Figure 3c). Under the same experimental conditions, Re–L–SiO_2 displayed slightly higher activity than Re–L. Similar effects of ligand derivatization were observed in our effort to covalently attach Co–cyclam onto SiO_2, as will be described later in Section 3.1.

Effects of derivatizing Re–bpy with amide groups have been investigated in CO_2–reduction electrocatalysis. Recently, Jia and co-workers[64] prepared a series of heterogenized Re(I) catalysts on Si electrode surfaces. It was shown that covalent linkages containing the amide groups were not stable under highly reducing conditions, while alkyl linkages were more stable.

2.3. Effects of Derivatizing the bpy Ligand at Different Positions

Another effect of ligand derivatization was also discovered through studying heterogenized Re–bpy.[65] In this case, the bpy ligand was derivatized at different positions prior to being coupled with a SiO_2 surface through a dipodal silane coupling agent and being coordinated with $Re(CO)_5Cl$. In particular, 2,2′–bipyridine–4,4′–dicarboxylic acid and 2,2′–bipyridine–5,5′–dicarboxylic acid were used to prepare surface–immobilized Re(I) catalysts following the synthesis described in Scheme 1b, resulting in the formation of Re–4–SiO_2 and Re–5–SiO_2,

respectively (see structures in Figure 4a). Both Re–4–SiO_2 and Re–5–SiO_2 exhibited a strong MLCT absorption band around 400 nm.[65]

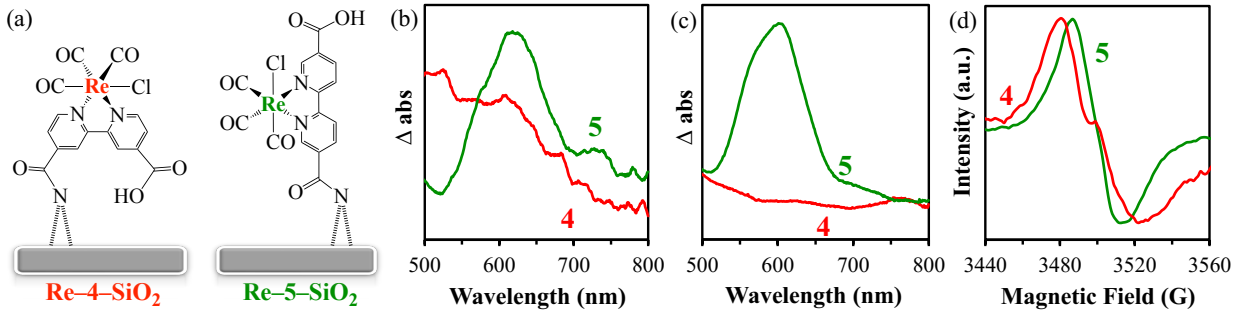

Figure 4. (a) Structures of Re–4–SiO_2 and Re–5–SiO_2, (b) difference UV-vis spectra of the two heterogenized Re(I) catalysts suspended in dimethylformamide, (c) difference UV-vis spectra of corresponding homogeneous Re(I) complexes in dimethylformamide, and (d) EPR spectra of the two heterogenized Re(I) catalysts in the powder form. Spectra in (b-d) were collected upon light irradiation at room temperature in the presence of TEOA and CO_2. Adapted with permission from *J. Mol. Catal. A* 2016, 411, 272-278. Copyright 2016 Elsevier.

During photocatalysis testing in the presence of triethanolamine (TEOA) as an electron donor, it was observed that the reaction suspension of Re–5–SiO_2 changed color from yellow to green. At room temperature, the green color gradually decayed over a few hours after the light was turned off, and re-appeared when light irradiation resumed.[65] In addition, the green color immediately changed back to yellow as soon as the reaction suspension was exposed to air under continuous light irradiation. Interestingly, such color change was not observed for Re–4–SiO_2. Spectroscopic studies indicated that this green color was associated with an absorption around 620 nm (Figure 4b). We further synthesized corresponding homogeneous complexes by coordinating 2,2′-bipyridine-4,4′-dicarboxylic acid and 2,2′-bipyridine-5,5′-dicarboxylic acid with $Re(CO)_5Cl$. A similar color change was observed for the Re(I) complex containing 2,2′-bipyridine-5,5′-dicarboxylic acid (Figure 4c) upon light irradiation. Under the experimental conditions, the Re–bpy complex will be reduced, forming a one–electron reduced species. The green color observed

for Re–5–SiO_2 is likely due to the electron density in the reduced Re–bpy being more localized on the 5,5′-derivatized bpy ligand, whereas in reduced Re–4–SiO_2 the electron density is more localized on the metal center.

This explanation was further supported by results obtained using electron paramagnetic resonance (EPR) spectroscopy.[65] In EPR studies, the heterogenized Re(I) catalysts in powder form was mixed with TEOA and purged with CO_2 prior to collecting EPR spectra. Figure 4d shows EPR spectra of Re–4–SiO_2 and Re–5–SiO_2 collected at room temperature and under continuous light irradiation. The spectrum of Re–4–SiO_2 shows some resonance features originated from hyperfine interactions between unpaired electrons with Re(I) nuclei (Figure 4d, red trace). Less significant hyperfine coupling features are seen in the spectrum of Re–5–SiO_2 (Figure 4d, green trace). Therefore, the electron density in reduced Re–5–SiO_2 is more localized on the bpy ligand while in reduced Re–4–SiO_2 the electron density is more localized on the metal center.

Effects of ligand derivatization at different positions were observed in a study by Argazzi and co-workers,[66] in which Ru(II) polypyridyl complexes were derivatized with –COOH groups for use in dye-sensitized solar cells. It was shown that moving the carboxylate moieties from the 4,4′-positions to the 5,5′-positions lowered the π^* energy of the bpy ligand. Subsequently, the Ru(II) photosensitizer containing 2,2′-bipyridine-5,5′-dicarboxylic acid was less efficient in converting photons into electrons because of more significant nonradiative decay of the excited states of this Ru(II) sensitizer. In a study by Guyot and co-workers,[67] carboxylic ester groups at the 5,5′-positions of the bpy ligand was found to have a drastic effect on the catalytic activity of Re–bpy toward electrochemical CO_2 reduction since the reducing equivalents are mainly accumulated on the electron-withdrawing ester, preventing the formation of Re(0) species and its interaction with CO_2. In comparison, alkyl-phosphonic ester substituents on the bpy ligand

preserved the catalytic activity of Re–bpy. In our study, derivatizing the bpy ligand at different positions led to difference in charge density distribution within the reduced Re(I) complexes. This difference contributed to the higher activity of Re–4–SiO_2 relative to Re–5–SiO_2 in photocatalytic CO_2 reduction.[65]

2.4. Effects of Surface Water

Some surface features could affect the structure, complexation, and behavior of heterogenized molecular catalysts. For example, Lian, Batista, and co-workers[68] demonstrated that the binding structure of Re–bpy catalysts can be significantly influenced not only by the nature and length of the covalent linkages, but also by the crystallographic facet of the surface. For our heterogenized molecular catalysts, the presence of surface water was found to have profound effects on the complexation of Re–bpy, while the presence of surface –OH groups dedicated the structure and activity of surface Co–cyclam (see Sections 3.1 and 3.2).

The infrared spectrum of Re–bpy in the molecular state contains three carbonyl bands in the 1900−2100 cm^{-1} range, corresponding to one high-energy, fully symmetric mode and two nearly degenerate lower-energy modes.[56, 69] The two lower-energy modes often coalesce to one broad feature, as seen in the DRIFTS spectrum of Re–L–SiO_2 (Figure 2d). These two modes can be resolved by exposing the heterogenized Re–bpy to TEOA and CO_2.[62] For example, three peaks at 2020, 1918, and 1896 cm^{-1} are present in the DRIFTS spectrum of Re–bpy covalently attached to a non-porous SiO_2 (Figure 5a). These absorption features are associated with the formation of a CO_2-bound Re(I) adduct, Re(I)–OOC–$OCH_2CH_2NR_2$ where R is CH_2CH_2OH, in the presence of TEOA and CO_2.[70] The Re(I)–OOC–$OCH_2CH_2NR_2$ species was suggested to be the real catalyst in many CO_2-reduction systems using diimine-tricarbonyl Re(I) complexes.

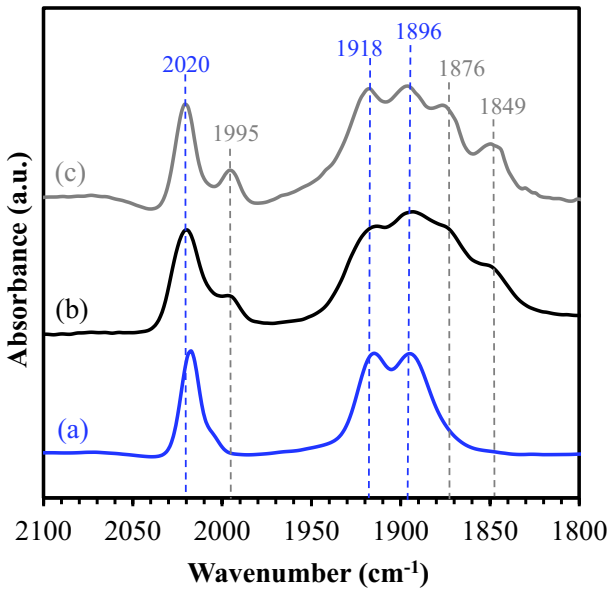

Figure 5. DRIFTS spectra of Re–bpy covalently attached to (a) a non-porous SiO_2, (b) a mesoporous SiO_2, and (c) Kaolin. The samples in the powder form were mixed with TEOA and exposed to air prior to spectra collection. Adapted with permission from *J. Mol. Catal. A* 2014, 395, 145-150. Copyright 2014 Elsevier.

Interestingly, another group of three peaks at 1995, 1876, and 1849 cm^{-1} are seen in the DRIFTS spectrum of Re–bpy covalently attached to a mesoporous SiO_2 (Figure 5b). These three peaks are more prominent in the spectrum of Re–bpy covalently attached Kaolin, a hydrated aluminum silicate (Figure 5c).[71] These peaks are associated with a surface Re(I)–OH species, formed upon replacing the Cl^- ligand on Re(I) with –OH, which could be produced by a reaction between TEOA and water (Reaction 1). The comparison shown in Figure 5 highlights the effect of surface water on the complexation of surface-immobilized Re–bpy. It was suggested that the presence of water in the interlayer space of Kaolin and mesopores of the mesoporous SiO_2 facilitated the formation of the Re(I)–OH species.[71]

$$(HOCH_2CH_2)_3N + H_2O \rightarrow (HOCH_2CH_2)_3NH^+ + OH^- \quad (1)$$

Interconversion between the surface Re(I)–OOC–$OCH_2CH_2NR_2$ and Re(I)–OH species was followed by DRIFTS. For example, conversion of Re(I)–OH to Re(I)–OOC–$OCH_2CH_2NR_2$ was observed under a flow of gaseous CO_2 in the presence of TEOA.[71] Under visible-light irradiation, the three peaks at 2020, 1918, and 1896 cm^{-1} shifted to lower wavenumbers, while the three peaks at 1995, 1876, and 1849 cm^{-1} did not shift but their intensities increased over time (Figure 6a). These observations indicate that the surface Re(I)–OOC–$OCH_2CH_2NR_2$ species was at least partially converted to the Re(I)–OH species, which is not photoactive and might be associated with the deactivation of the heterogenized Re–bpy. Figure 6b summarizes possible reactions of different surface Re(I) species based on DRIFTS studies. Our studies suggest that the presence of surface water has a strong impact on the complexation and even photoactivity of surface Re–bpy.

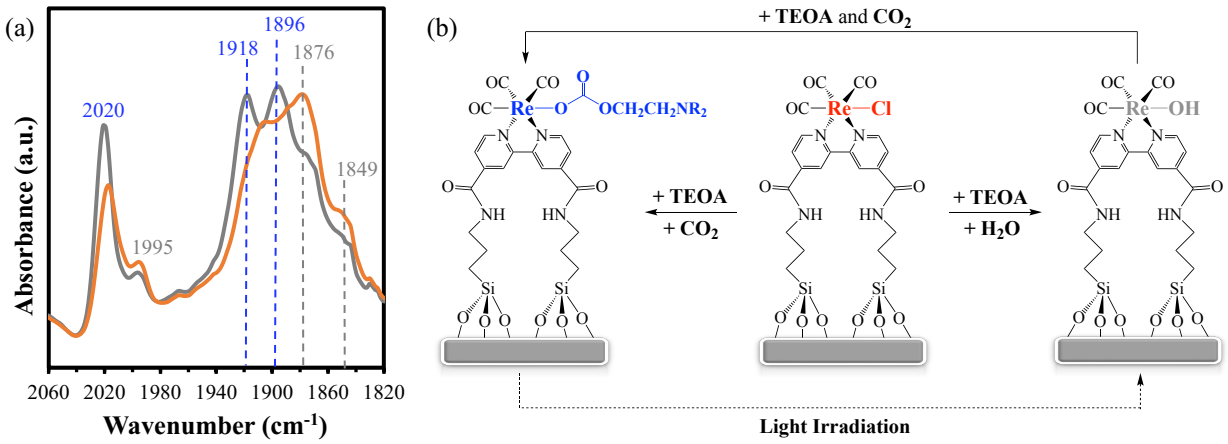

Figure 6. (a) DRIFTS spectra of Re–bpy covalently attached to Kaolin before (gray) and after (orange) light irradiation in the presence of TEOA. (b) Possible pathways for the formation of different surface Re(I) complexes; R = CH_2CH_2OH. Adapted with permission from *J. Mol. Catal. A* 2014, 395, 145-150. Copyright 2014 Elsevier.

3. Heterogenization of Co–cyclam for Visible-light CO_2 Reduction

In addition to Re–bpy, other molecular catalysts have been covalently attached onto semiconductor surfaces for use in light-driven CO_2 reduction.[72-79] Among these heterogenized molecular catalysts, many employed cobalt complexes because of their outstanding performance, low cost, and reasonable stability. Our research in this direction aims at achieving visible-light CO_2 reduction using heterogenized Co–cyclam on semiconductor surfaces. Co–cyclam demonstrated excellent activity in selective CO_2-to-CO conversion in the presence of a molecular photosensitizer, *p*-terphenyl, under UV irradiation (Scheme 2a). A serendipitous finding led to the deposition of Co–cyclam on SiO_2 via an oxo bridge (Scheme 2b). The resulting heterogenized Co–cyclam demonstrated better activity than the molecular Co–cyclam in CO_2 reduction under the same conditions. Co–cyclam was then deposited on TiO_2 (Scheme 2c) and C_3N_4 (Scheme 2d) which replaced *p*-terphenyl as the photosensitizers in CO_2. Our research also revealed the effects of ligand derivatization and surface –OH groups on the structure and activity of heterogenized Co–cyclam. This line of research further inspired us to synthesize a Co SAC on C_3N_4 which showed excellent activity in visible-light CO_2 reduction (see Section 4).

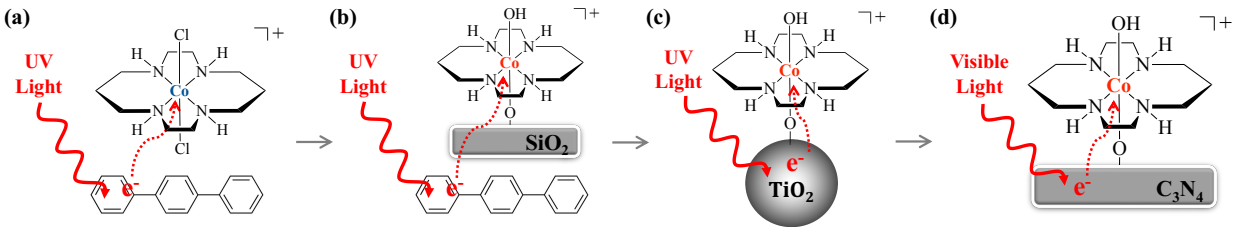

Scheme 2. Our research approach to obtain heterogenized Co–cyclam for visible–light CO_2 reduction.

3.1. Surface Immobilization of Co–cyclam on SiO_2

Sujandi and co-workers prepared Co–cyclam covalently attached onto mesoporous SiO_2 through N-functionalization of the cyclam ligand.[80] The resulting catalyst showed good activity in

aerial oxidation of ethylbenzene. In our synthesis of heterogenized Co–cyclam, the SiO_2 surface was initially functionalized with a bromo silane coupling agent (Scheme 3, left). Cyclam-functionalized SiO_2 was then prepared by reacting bromo-functionalized SiO_2 with cyclam in the presence of triethylamine (TEA). Heterogenized Co–cyclam, denoted "Co–L–SiO_2", was obtained as a green powder after reacting $CoCl_2$ with cyclam–functionalized SiO_2 in the presence of oxygen.[81] The UV-vis spectrum of Co–L–SiO_2 features a distinct peak around 630 nm (Figure 7, solid trace), characteristic of the *trans* isomer of Co–cyclam (Figure 7, dotted trace).[82]

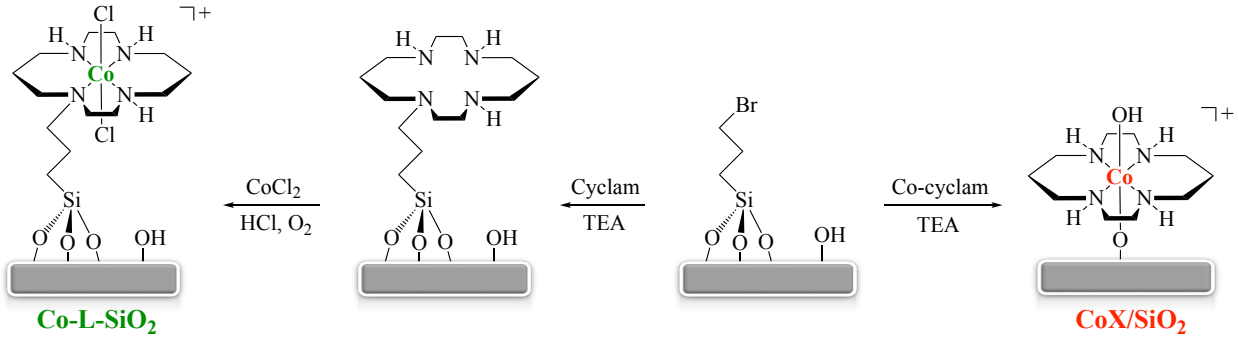

Scheme 3. Synthetic routes to obtain Co–L–SiO_2 (left) and CoX/SiO_2 (right). TEA: triethylamine.

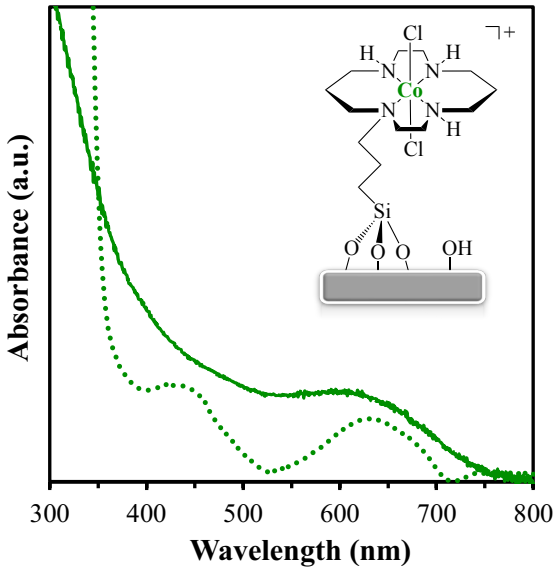

Figure 7. UV–vis spectra of Co–L–SiO_2 in the powder form (solid trace) and Co–cyclam in H_2O (dotted trace). Adapted with permission from *J. Coord. Chem.* 2016, 69, 1748-1758. Copyright 2016 Taylor & Francis Group.

The synthesized Co–L–SiO_2 was tested in photocatalytic CO_2 reduction using *p*-terphenyl as a molecular photosensitizer. Both CO and H_2 were detected as the major products in the presence of TEOA and methanol as electron donors. Under the same experimental condition, Co–L–SiO_2 demonstrated significantly lower activity and selectivity towards CO formation than Co–cyclam.[81] A turnover number (TON) of 12.5 for CO formation was obtained using Co–L–SiO_2 after CO_2 reduction for 4 h, compared to 141.8 for Co–cyclam. The selectivity towards CO formation, as measured by the CO/H_2 ratio, was determined to be 7.8 and 15.1 for Co–L–SiO_2 and Co–cyclam, respectively. These results indicate that heterogenization through N-functionalization (Scheme 3, left) was detrimental to the catalytic property of Co–cyclam. In a study by Froehlich and co-workers,[83] a similar effect was observed in electrochemical CO_2 reduction using homogeneous Ni(II) cyclam catalysts, where N-functionalization on cyclam with methyl groups drastically altered the redox and catalytic properties of Ni(II) cyclam. Therefore, the observed detrimental effect originated from derivatizing one of the amines on the cyclam ring. Such a detrimental effect could be avoided by derivatizing on one of the C atoms of the cyclam ligand for surface immobilization. Recently, Forget and co-workers[84] prepared C-functionalized Ni(II) cyclam grafted onto a carbon electrode. The resulting catalyst demonstrated excellent activity in electrochemical CO_2 reduction.

In another attempt to synthesize Co–L–SiO_2, Co–cyclam was mixed directly with bromo-functionalized SiO_2 in the presence of TEA (Scheme 3, right). Interestingly, this reaction resulted in the formation of a different catalyst, denoted "CoX/SiO_2", in which the Co(III) center is directly deposited on SiO_2 via an oxo bridge. Further characterization of CoX/SiO_2 suggested that the

chloro ligands in Co–cyclam was replaced with –OH ligands upon surface deposition.[81] Likely, Co–cyclam reacted preferentially with surface silanol (Si–OH) groups, instead of the bromo groups, on the functionalized SiO_2. Based on this discovery, we employed a microwave-assisted synthesis to achieve uniform deposition of Co–cyclam on an unfunctionalized mesoporous SiO_2.[85] The resulting CoX/SiO_2 demonstrated superior activity in CO_2 reduction using *p*-terphenyl as a photosensitizer. A TON more than 300 was obtained for CO after photocatalytic CO_2 reduction for 4 h (Figure 8).

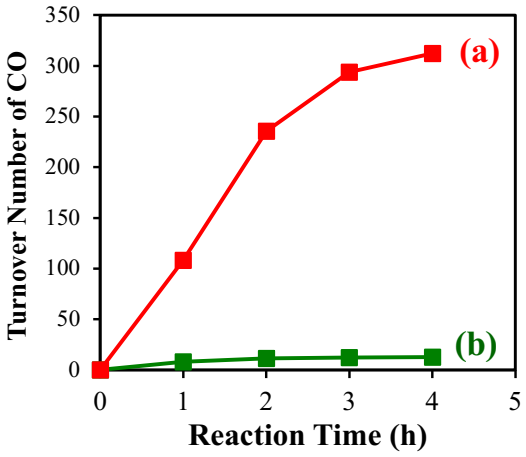

Figure 8. Photocatalytic CO_2 reduction using (a) CoX/SiO_2 and (b) Co–L–SiO_2. The reaction was carried out using *p*–terphenyl as a photosensitizer and TEOA and methanol as electron donors. Adapted with permission from *J. Coord. Chem.* 2016, 69, 1748-1758. Copyright 2016 Taylor & Francis Group.

In order to further probe the structure of CoX on surfaces, Co–cyclam was deposited via the microwave method on a mesoporous SiO_2 with a surface area of 569 m^2/g and a non-porous SiO_2 with a surface area of 200 m^2/g. Under the same synthetic conditions, CoX deposited on the mesoporous SiO_2 (cobalt loading 19 μmol/g) displayed a green color, corresponding to three absorptions at 600 nm, ~460 nm, and ~380 nm in its UV-vis spectrum (Figure 9a). In contrast,

CoX deposited on the nonporous SiO_2 (cobalt loading 13 μmol/g) had a brown color, and the three peaks are not distinguishable in its UV-vis spectrum due to peak broadening and overlapping (Figure 9b). Likely, CoX exists on the nonporous SiO_2 as a peroxo Co(III) complex featuring a Co–O_2–Co unit.[86] In photocatalytic CO_2 reduction using *p*-terphenyl as the photosensitizer, CoX on the mesoporous SiO_2 demonstrated significantly higher activity than on the nonporous SiO_2.

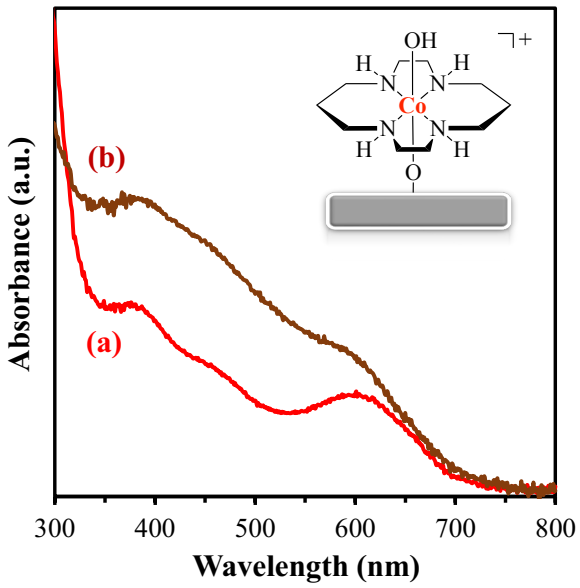

Figure 9. UV-vis spectra of CoX deposited on (a) a mesoporous SiO_2 and (b) a non-porous SiO_2 via the microwave method. Adapted with permission from *Dalton Trans.* 2017, 46, 10721-10726. Copyright 2017 Royal Society of Chemistry.

3.2. Deposition of Co–cyclam on TiO_2

Following the same microwave synthesis, CoX was deposited on TiO_2 (Scheme 2c) in order the eliminate the use of molecular photosensitizers such as *p*-terphenyl.[87] Upon UV light irradiation, photoexcited electrons in TiO_2 nanoparticles were transferred to the surface CoX for CO_2 reduction. On the surface of a commercial TiO_2 material, Evonik P25 consisting of ~80% anatase and ~20% rutile, a TON of 11.2 for CO production was obtained in photocatalytic CO_2

reduction in the presence of TEOA as the electron donor (Figure 10a). In comparison, no significant CO production was observed using a suspension containing P25 TiO_2 nanoparticles and Co–cyclam.

The presence of certain surface –OH groups on TiO_2 was found to be essential for the molecular deposition of Co–cyclam.[88] We prepared two photocatalysts, CoX/P25 and CoX/Rutile, which were prepared by depositing CoX on two commercial TiO_2 materials, P25 and Rutile nanopowder (Sigma-Aldrich), respectively. In photocatalytic CO_2 reduction, CoX/P25 exhibited very good activity, while negligible CO production was observed using CoX/Rutile (Figure 10). DRIFTS studies indicated the presence of terminal Ti–OH groups on P25, while the surface of Rutile lacked such –OH groups. In a study by Petsi and co-workers,[89] surface –OH groups were found to be important for the deposition of $[Co(H_2O)_6]^{2+}$ on TiO_2 nanoparticles. In our study, the terminal –OH groups are likely essential for the molecular deposition of catalytically active CoX on P25 via Ti–O–Co linkages. The lack of sufficient Ti–O–Co linkages in CoX/Rutile led to inefficient photoexcited electron transfer from Rutile to surface CoX, resulting in its poor activity in photocatalytic CO_2 reduction (Figure 10b).

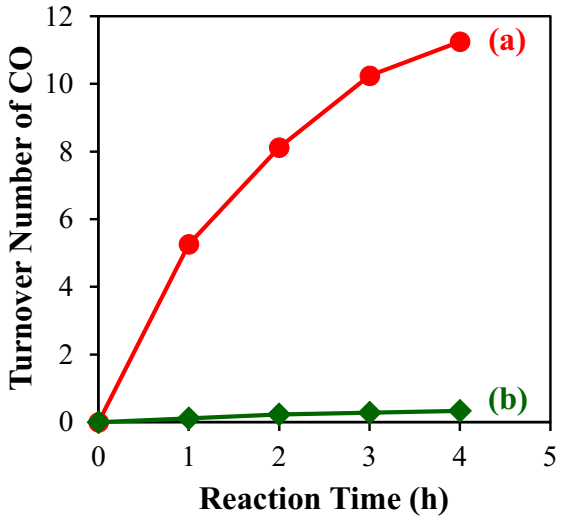

Figure 10. Photocatalytic CO_2 reduction using (a) CoX/P25 and (b) CoX/Rutile. The reaction was carried out under UV light using TEOA as an electron donor. Adapted with permission from *J. Mol. Catal. A* 2016, 423, 293-299. Copyright 2016 Elsevier.

Additional characterization confirmed that CoX exists in different forms on CoX/P25 than on CoX/Rutile. For example, the UV-vis spectrum of CoX/P25 contains two broad absorptions at ~460 nm and 600 nm (Figure 11a), indicating the presence of uniform, molecularly deposited CoX.[88] However, these features are absent in the spectrum of CoX/Rutile (Figure 11b). Microscopic images showed that amorphous, nano-sized aggregates of CoX are present in CoX/Rutile, but not in CoX/P25.

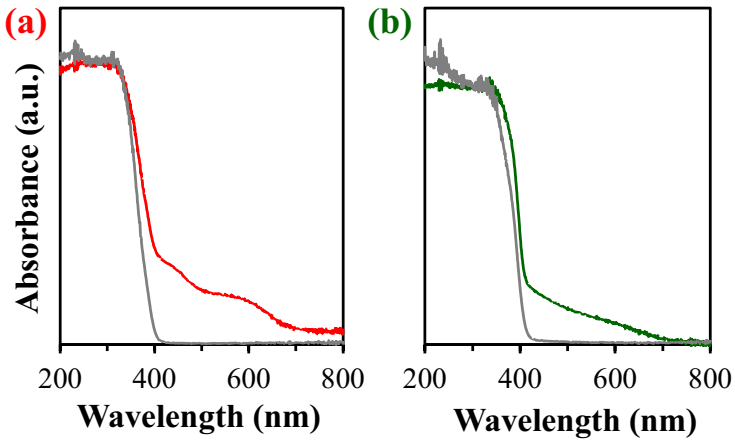

Figure 11. UV-vis spectra of (a) CoX/P25 and (b) CoX/Rutile. The spectra of bare P25 and Rutile are included as gray traces. Adapted with permission from *J. Mol. Catal. A* 2016, 423, 293-299. Copyright 2016 Elsevier.

Based on the specific surface areas of the TiO_2 materials and elemental analysis results, surface catalyst densities were estimated to be 6-7 Co per nm^2 surface in CoX/P25 and ~26 Co per nm^2 surface in CoX/Rutile.[88] These numbers further support our conclusion that CoX is molecularly deposited on P25. The absence of terminal –OH groups for uniform deposition of CoX

on Rutile resulted in the formation of CoX in the aggregated form as observed in microscopic images.

Characterization with EPR spectroscopy confirmed the fact that surface cobalt sites exist in different states on Rutile than on P25. Upon deposition on TiO_2 surface in the presence of TEA, some Co(III) centers were reduced to Co(II), which served as a sensitive probe for EPR studies.[88] As shown in Figure 12, the spectrum of CoX/P25 under N_2 (Figure 12a, gray trace) contains resonances corresponding to mononuclear high-spin Co(II) ($S = 3/2$) centers at $g_x = 5.89$, $g_y = 3.40$, and $g_z = 2.22$ (not labeled). The same spectrum also contains resonances near $g = 2$ (not labeled) that are associated with trapped electrons and holes in P25[90, 91] upon exposure to ambient light.

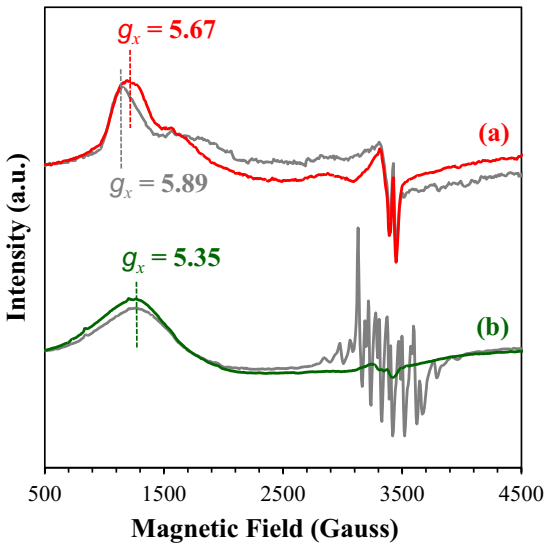

Figure 12. X-band EPR spectra of (a) CoX/P25 and (b) CoX/Rutile under CO_2. Corresponding spectra under N_2 are also included (gray traces). The spectra were collected at liquid He temperature after purging the samples under N_2 or CO_2 at room temperature. Adapted with permission from *J. Mol. Catal. A* 2016, 423, 293-299. Copyright 2016 Elsevier.

In the spectrum of CoX/Rutile (Figure 12b, gray trace), however, a very different EPR spectrum was observed in the high-spin region featuring a broad Co(II) peak with $g = 5.35$ due to

averaging of g_x and g_y components indicative of Co(II) in a broad range of coordination geometries. In addition, strong eight-line signals associated with oxygen-centered radicals were observed in the region of $g = 2$. Likely, some of the CoX exists as a peroxo complex featuring a Co–O_2–Co unit on Rutile, similar to that on the nonporous SiO_2 (Figure 9).

Upon CO_2 adsorption, the Co(II) sites in CoX/P25 displayed a high-spin signal at $g_x = 5.67$ (Figure 12a), indicating that the adsorbed CO_2 on CoX/P25 took electron density away from the Co(II) centers. On CoX/Rutile (Figure 12b), CO_2 adsorption did not shift the high-spin Co(II) signal at $g_x = 5.35$. Instead, the hyperfine splitting of the oxygen radicals vanished and an anisotropic signal appeared near $g = 2$ (not labeled). This observation implies that the electron density on the oxygen radicals adjacent to Co(II) was preferentially transferred to CO_2 and adsorption of CO_2, in fact, removed electron exchange of Co(II) with oxygen atoms on the Rutile surface. Based on these observations, it can be concluded that the Co(II) sites in CoX/Rutile are in a broad range of coordination geometries different than those in CoX/P25.

3.3. Deposition of Co–cyclam on C_3N_4

An inorganic polymeric semiconductor, C_3N_4 has attracted enormous interest due to its low cost, high thermal and chemical stability, nitrogen-rich structure, and suitable bandgap (2.7 eV).[92-94] In CO_2 reduction, C_3N_4-based materials have been employed as photocatalysts [95-97] or coupled with metal-ligand complexes[76-79, 98-104] to achieve enhanced catalysis. For example, Roy and co-workers[76] deposited cobalt phthalocyanine cyanine on mesoporous C_3N_4 via a weak π-π stacking interaction for visible-light CO_2 reduction. Wei and co-workers[79] attached a cobalt quaterpyridine complex onto C_3N_4 through an amide linkage, which showed remarkable selectivity (98%) towards CO production under visible-light irradiation. In the recent work by Shang and co-workers,[104] a

cobalt phthalocyanine complex was deposited on C_3N_4 for photocatalytic CO_2 reduction. The cobalt phthalocyanine complex contains –COOH groups, which enabled high surface coverage of the cobalt complex and promoted its catalytic property.

In our study, Co–cyclam was deposited on C_3N_4 (Scheme 2d) in the presence of TEA, forming CoX/C_3N_4 as indicated by a broad peak around ~600 nm in its UV-vis spectrum (Figure 13). A TON of more than 160 for CO production was obtained using Co–cyclam deposited on a modified C_3N_4 after CO_2 reduction for an extended period under visible–light irradiation ($\lambda > 420$ nm).[105] Under the same reaction condition, no CO was produced using a physical mixture of Co–cyclam and C_3N_4.

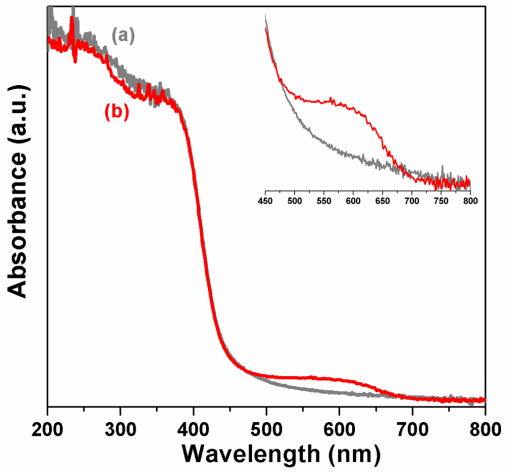

Figure 13. UV–vis spectra of (a) bare C_3N_4 and (b) CoX/C_3N_4. Insert: a close view of the spectra.

In combination with computational modeling, X-ray absorption spectroscopy (XAS) was employed to investigate the structure of CoX on C_3N_4.[105, 106] For metal-based catalytic materials, the extended X-ray absorption fine structure (EXAFS) analysis can provide valuable insights into the local geometric structure and coordination environment of the metal sites,[107] while the X-ray absorption near edge structure (XANES) spectroscopy is particularly sensitive to the electronic

structure of the metal center and its local environment.[108] As can be seen in Figure 14a, the Co K-edge XANES spectrum of CoX/C_3N_4 has different features than that of Co–cyclam, confirming that the coordination environment of cobalt significantly changed upon deposition on C_3N_4. Based on prior studies,[87, 88, 101] we hypothesize that the two axial Cl ligands of Co–cyclam were replaced with one OH group and one surface –O– or –NH– group upon deposition on C_3N_4 in the presence of TEA.

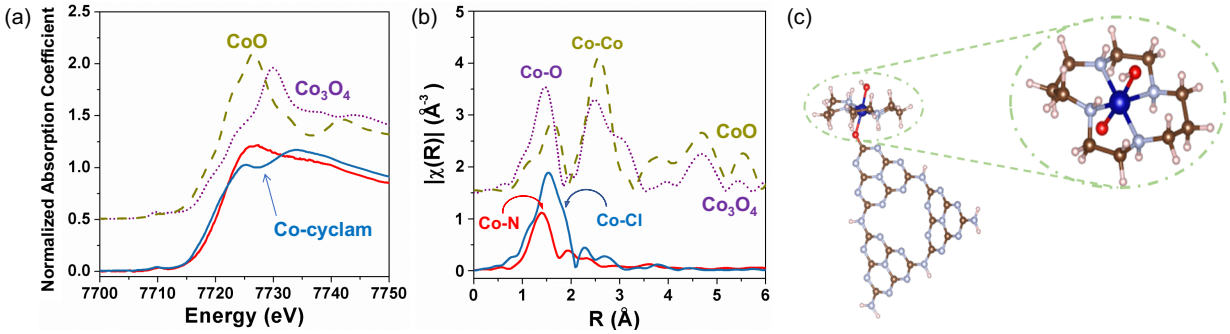

Figure 14. (a) XANES and (b) EXAFS spectra of Co–cyclam (blue), CoX/C_3N_4 (red), and CoO and Co_3O_4 as references. (c) An optimized structure of CoX attached to C_3N_4 through an oxygen atom. Color scheme: Co (blue), N (silver), C (brown), O (red), and H (pink). Adapted with permission from *J. Phys. Chem. C* 2023, 127, 3626-3633. Copyright 2023 American Chemical Society.

Our hypothesis was supported by the Co K-edge EXAFS spectra of Co–cyclam and CoX/C_3N_4 (Figure 14b), which clearly indicate the absence of Co–Cl bonds in CoX/C_3N_4. Fitting the first peak of the EXAFS spectrum of Co–cyclam led to coordination numbers of 3.5±1.2 and 2.0±1.2 for Co–N and Co–Cl bonds, respectively. The Co–O scattering path was chosen to fit the first peak of CoX/C_3N_4, resulting in a coordination number of 6.3±1.4 for Co–O nearest neighbors.[105] Since the bond lengths of Co–N and Co–O are very close to each other, our experimental results were not able to distinguish between contributions from N and O atoms. We further carried out density functional theory (DFT) simulations, in which anchoring of CoX to

C_3N_4 through either a surface –O– or –NH– group represents the most probable modes. Similar energies and distances between the Co center of CoX and C_3N_4 were obtained for these two modes. Therefore, it remains unclear whether CoX attaches to C_3N_4 through the –O– or –NH– group. Nevertheless, the structure shown in Scheme 2d represents a plausible model of CoX/C_3N_4. Figure 14c shows a DFT optimized structure of CoX attached to C_3N_4 through an oxygen atom.

A similar macrocyclic complex, [Co(HMD)Cl_2]Cl where HMD is 5,7,7,12,14,14-hexamethyl-1,4,8,11-tetraazacyclotetradeca-4,11-diene, is also known for its catalytic activity in selective CO_2 reduction.[109] We have deposited this cobalt complex onto different semiconductor surfaces (TiO_2, N-Ta_2O_5, and C_3N_4). The resulting heterogenized catalyst on TiO_2 demonstrated lower activity than CoX/TiO_2 in CO_2 reduction under UV irradiation, while on C_3N_4 it showed significantly higher activity than CoX/C_3N_4 under visible-light irradiation.[101]

4. Single Atom Catalysts in C_3N_4 for Visible-light CO_2 Reduction

Crystalline porous materials, particularly metal-organic frameworks (MOFs), are excellent support for constructing well-defined catalytic sites.[110-112] A variety of molecular catalysts, including Re–bpy, have been incorporated in MOFs with demonstrated activity towards photocatalytic CO_2 reduction.[113-116] Other examples of such catalysts in porous materials include metal-to-metal charge transfer units[117-119] and single atom catalysts (SACs).[120-123] Porous materials represent an ideal platform for studying effects of chemical microenvironment on the activity of well-defined catalytic sites.[124-126]

SACs have been extensively explored in a variety of applications including photocatalytic[44-48] and electrocatalytic CO_2 reduction.[127-129] Two-dimensional materials, including N-doped graphene and C_3N_4, have been employed as the support for SACs.[130-132] The N-rich

framework of C_3N_4 enables it to serve as a photoactive support for SACs featuring metal (M)–N coordination.[133-135] In 2018, we reported a Co SAC on C_3N_4 that demonstrated interesting activity in selective CO_2 reduction under visible-light irradiation.[136] Since then, many studies have examined SACs on C_3N_4 for solar CO_2 reduction.[137-151] For example, Wang and co-workers[149] synthesized an Ni SAC anchored by boron–oxo species on C_3N_4 nanosheets. The Ni SAC was shown to possess a unique Ni–O_6 coordination and demonstrated excellent activity towards CO and CH_4 production in photocatalytic CO_2 reduction. Sun and co-workers[150] prepared two Cu SACs with different Cu configurations (Cu_1N_3 and Cu_1P_3) on phosphorus-doped C_3N_4. In visible-light CO_2 reduction in the presence of H_2O, the Cu SAC containing the Cu_1N_3 unit was found to be active towards CO production, while the Cu SAC containing the Cu_1P_3 unit preferentially produced H_2 instead of CO. Ou and co-workers[151] synthesized a SAC with two active centers, Mn and Co, on C_3N_4. Experimental results and DFT calculations showed an interesting synergy in photocatalysis using the Mn-Co SAC, where H_2O oxidation occurred on the Mn center and CO_2 reduction occurred on the Co center.

In 2016, Gao and co-workers[152] predicted that efficient visible-light CO_2 reduction can be achieved using single Pd and Pt atoms supported on C_3N_4. Inspired by this report and other prior work on SACs, we prepared a Co SAC on C_3N_4 (Figure 15a) by mixing $CoCl_2$ with C_3N_4 in acetonitrile, followed by microwave heating in the presence of TEA.[136] The typical SAC behavior was observed in photocatalytic CO_2 reduction using the synthesized material (Figure 15b). At relatively low cobalt loadings, the presence of single Co^{2+} sites was confirmed with XAS (Figure 15c, red trace). Catalytically inactive cobalt oxide nanoparticles were produced at high cobalt loadings (Figure 15c, blue trace).

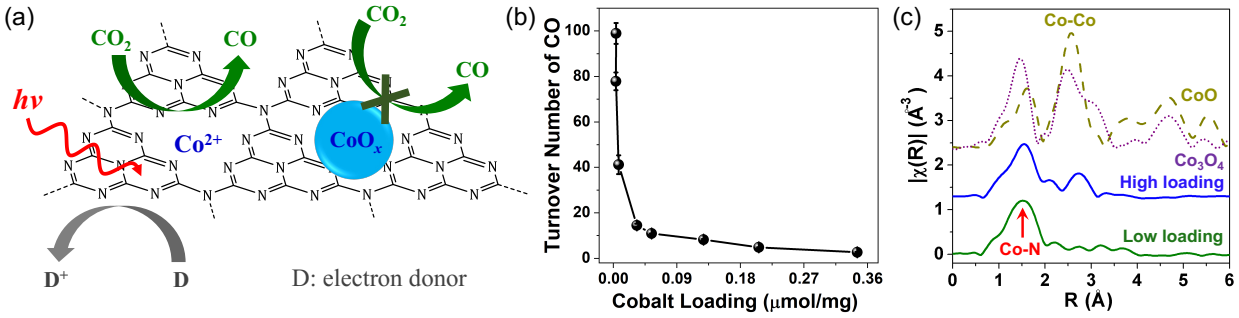

Figure 15. (a) Schematic of photocatalytic CO_2 reduction mediated by a Co SAC on C_3N_4; (b) TONs of CO after CO_2 reduction for 2 h as a function of cobalt loading; (c) EXAFS spectra of Co^{2+} on C_3N_4 at low and high loadings, and CoO and Co_3O_4 as references. Adapted with permission from *J. Am. Chem. Soc.* 2018, 140, 16042-16047. Copyright 2018 American Chemical Society.

Different structural modes have been proposed for SACs on C_3N_4, including in-plane M–N_3 and inter-layer M–N_4 coordination,[153] C–M–N_2 coordination,[137] M–N_4 coordination in the presence of N vacancies,[154] and other possibilities.[155, 156] Results from fitting the EXAFS spectrum shown in Figure 15c indicated that our Co SAC has four equivalent Co–N bonds. However, computational modeling failed to reach such a Co–N_4 structure inside the "pocket" of pristine C_3N_4 (Figure 16, a and b). Instead, a Co–N_{2+2} coordination at C_3N_4 edge sites appeared to be the most probable structure (Figure 16c).[157] For this structure, the calculated Co–N bond length is in the range of 2.07-2.10 Å, in excellent agreement with the value ($d_{Co–N}$ 2.08 Å) obtained by fitting the EXAFS spectrum. This mode of coordination was further supported by our experimental results obtained using a Co SAC in C_3N_4 treated with NH_3, which contains more edge sites than untreated C_3N_4 and subsequently allows a significantly higher loading of single Co^{2+} sites. Similar SAC structures have been reported, such as the Fe–N_{2+2} sites of Fe SACs confined in N-doped carbon materials.[129, 158, 159]

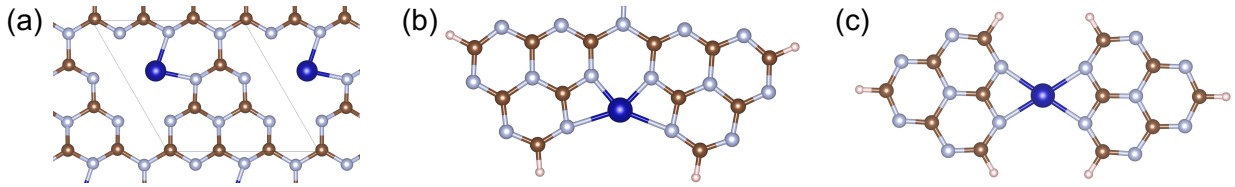

Figure 16. Structure models of single Co^{2+} sites coordinated with N atoms in C_3N_4: (a) $Co{-}N_2$, (b) $Co{-}N_4$, and (c) $Co{-}N_{2+2}$ at edge sites. A 4 × 4 × 1 k-point mesh and a force convergence of 10^{-5} eV/Ang was used in modeling studies. Color scheme: Co (blue), N (silver), C (gold), and H (light brown). Adapted with permission from *J. Phys. Chem. C* 2022, 126, 8596-8604. Copyright 2022 American Chemical Society.

Doping C_3N_4 with an appropriate amount of carbon significantly enhanced the photocatalytic activity of the Co SAC on C_3N_4.[160] In our study, carbon doping was achieved by adding a small amount of dextrose to urea (5-400 mg dextrose per 20 g urea) for synthesizing C_3N_4 via pyrolysis. Figure 17a shows the pictures of synthesized C_3N_4 containing varying amounts of carbon dopant. While pristine C_3N_4 synthesized from pure urea displays a light yellow color, C-doped C_3N_4 becomes darker in color with increasing amounts of dextrose used in synthesis. These C_3N_4 materials were used to prepare Co SACs following our established method, which was then tested in photocatalytic CO_2 reduction to probe the effect of carbon doping. As can be seen from Figure 17b, an optimal level of carbon doping exists since the highest activity was obtained using a Co SAC on a C-doped C_3N_4 material synthesized from 20 mg dextrose and 20 g urea. In subsequent studies, this particular C-doped C_3N_4 was utilized to prepare Co SACs.

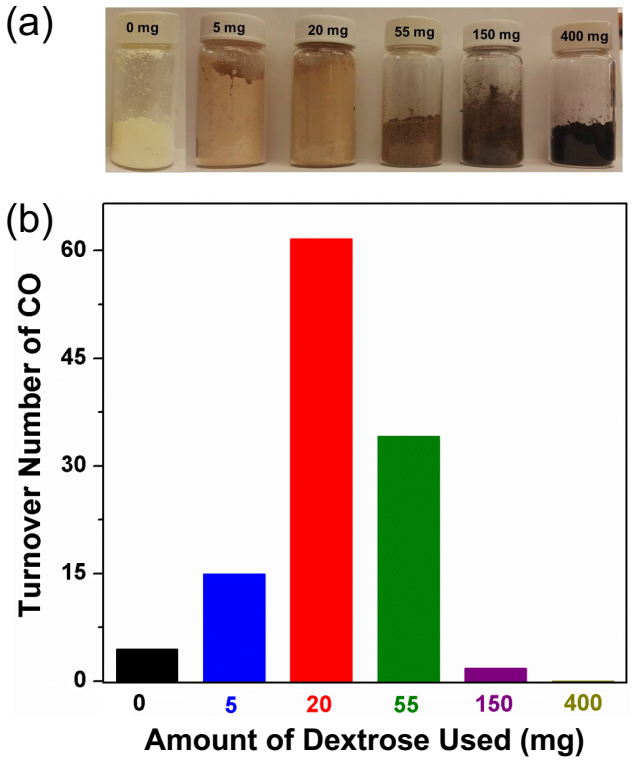

Figure 17. (a) Pictures of C_3N_4 synthesized in the presence of different amounts of dextrose. (b) TONs for CO production after photocatalytic CO_2 reduction for 2 h using Co SACs on different C-doped C_3N_4. Adapted with permission from *ChemNanoMat* 2021, 7, 1051-1056. Copyright 2021 Asian Chemical Editorial Society.

At a cobalt loading ~0.014 μmol/mg, TONs of 4.4 and 61.6 for CO production were obtained using a Co SAC on pristine C_3N_4 (denoted "Co^{2+}@C_3N_4") and a Co SAC on C-doped C_3N_4 (denoted "Co^{2+}@C-C_3N_4"), respectively (Figure 18a).[157] The XANES spectrum of Co^{2+}@C_3N_4 is almost identical to that of Co^{2+}@C-C_3N_4 (Figure 18b), suggesting that the two Co SACs have similar electronic and geometric structures. Additional characterization was done to explore possible reasons for the observed enhancement in photocatalysis. The synthesized C-C_3N_4 has greater absorption than pristine C_3N_4 in the visible-light region (400-800 nm, Figure 18c). The different photoluminescence spectra of C-C_3N_4 and C_3N_4 (Figure 18d) indicate that doping C_3N_4 with carbon significantly inhibited photoinduced charge recombination. It has been reported that appropriate carbon doping can enhance the photocatalytic properties of C_3N_4 materials by

improving its photoresponse and inhibiting charge recombination.[161] These factors should account for, at least partly, the observed higher activity of Co^{2+}@C-C_3N_4 than Co^{2+}@C_3N_4 in our study.

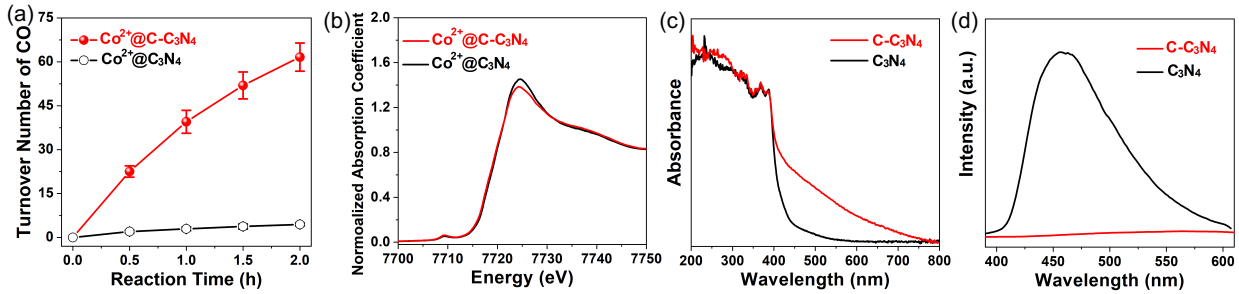

Figure 18. Pristine C_3N_4 versus C-doped C_3N_4: (a) CO production in photocatalytic CO_2 reduction using Co SACs, (b) normalized Co K-edge XANES spectra of Co SACs and reference samples (CoO and Co_3O_4); (c) optical absorption, and (d) photoluminescence spectra. Adapted with permission from *J. Phys. Chem. C* 2022, 126, 8596-8604. Copyright 2022 American Chemical Society.

Our experimental results suggest that other factors also contributed to the enhanced activity of Co^{2+}@C-C_3N_4 in photocatalytic CO_2 reduction. In particular, Co–cyclam deposited on C-C_3N_4 displayed a 2-fold enhancement in activity in comparison with Co–cyclam deposited on C_3N_4 (CoX/C_3N_4 in Section 3.3).[157] Under the same experimental condition, Co^{2+}@C-C_3N_4 demonstrated ~14 times higher activity than Co^{2+}@C_3N_4 in CO_2 reduction. Therefore, C doping likely also affected the coordination environment of Co^{2+} sites in C-C_3N_4. In our study, the Co–N_{2+2} coordination at C_3N_4 edge sites is also the most probable structure for Co^{2+}@C-C_3N_4. A simplified model of C doping was proposed to explore possible additional effects of C doping. In this model, the presence of C dopant near the cobalt centers (Figure 19, circled in red) results in shorter Co–N bond length and stronger Co–N binding energy. In addition to enhanced light absorption and charge separation in C-doped C_3N_4, the stronger Co–N binding upon C doping likely contributes to the improved catalytic properties of Co^{2+}@C-C_3N_4.

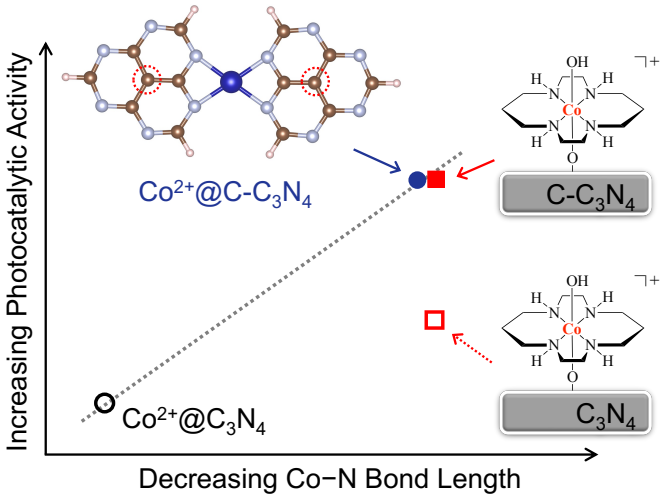

Figure 19. A proposed correlation between observed photocatalytic activity and calculated Co–N bond length of Co^{2+}@C_3N_4, Co^{2+}@C-C_3N_4, CoX/C_3N_4, and CoX/C-C_3N_4. In the model of Co^{2+}@C-C_3N_4, two of the framework N atoms are replaced with C atoms (circled in red). Color scheme: Co (blue), N (silver), C (gold), and H (light brown).

It is much desired to obtain unified structure-property relationships for different catalytic materials.[162] In our research, the Co–N_4 unit is crucial for the CO_2-reduction activity of both the heterogenized Co–cyclam and the Co SAC on C_3N_4. The calculated Co–N bond length in Co^{2+}@C-C_3N_4 (1.96-1.97 Å) is very close to that in Co–cyclam (1.97-2.02 Å).[157] It is possible that insights learned from studying such SACs could serve as inspiration for the design and development of innovative molecular catalysts, and vice versa.

5. Summary and Outlook

Heterogenized molecular catalysts and SACs contain well-defined surface catalytic sites. They have demonstrated exciting activities in various applications, including solar CO_2 reduction. Our recent research has focused on (i) covalently attaching two well-known molecular catalysts, Re–bpy and Co–cyclam, on different surfaces, and (ii) understanding the structures of Co SACs on C_3N_4. We have utilized catalyst synthesis, spectroscopic characterization, and computation

modeling to interrogate the structures of well-defined surface catalytic sites and understand factors affecting their structures and photocatalytic activities.

In particular, Re–bpy was covalently grafted onto SiO_2 surfaces via amide linkages. Derivatization of the bpy ligand with electron-withdrawing amide groups significantly lowered the activity of Re–bpy in photocatalytic CO_2 reduction. Such derivatization at different positions of the bpy ligand resulted in electron density being localized in different parts of Re–bpy upon photoreduction and subsequently different photocatalytic activity. The presence of surface water was found to have a strong impact on the complexation and even photoactivity of surface Re–bpy.

Similar effects of ligand derivatization and surface characteristics were observed in heterogenization of Co–cyclam on different surfaces. In the presence of *p*-terphenyl as a molecular photosensitizer, Co–cyclam grafted onto SiO_2 via one of the coordinating N atoms showed poor activity towards CO_2 reduction. Under the same experimental conditions, Co–cyclam directly deposited on SiO_2 via an oxo bridge on the Co center demonstrated excellent activity. This oxo bridge strategy was employed to deposit Co–cyclam on TiO_2, which functioned as a light absorber in photocatalysis, eliminating the need for *p*-terphenyl as a molecular photosensitizer. The presence of surface OH groups on SiO_2 and TiO_2 was found to be key for the effective surface deposition of Co–cyclam. Building on these results, visible-light CO_2 reduction was achieved using Co–cyclam deposited C_3N_4, which has a narrower bandgap than TiO_2 and can be activated under visible-light irradiation.

Inspired by the activity of Co–cyclam on C_3N_4 and prior work on SACs by others, we discovered a Co SAC featuring Co^{2+} coordinated to framework N atoms on C_3N_4. The Co SAC demonstrated excellent activity in visible-light CO_2 reduction. Based on spectroscopic and modeling studies, a Co–N_{2+2} coordination at C_3N_4 edge sites was suggested to be the most probable

structure. Doping C_3N_4 with an appropriate amount of carbon significantly enhanced the photocatalytic activity of the Co SAC. A model of carbon doping was also proposed, which involves the substitution of N atoms near the Co centers with C atoms.

In our research, spectroscopic techniques, including infrared, UV-visible, electron paramagnetic resonance, and X-ray absorption spectroscopies, were extensively utilized to understand the structures and properties of heterogenized molecular catalysts and SACs. Computational modeling further provided important insights regarding the structures of these well-defined surface catalytic sites at the molecular level. Our research has been largely inspired by exciting research results from other groups, some of which are briefly discussed in this article. Needless to say, many questions remain unanswered as we continue to investigate these photocatalytic materials.

Despite the tremendous progress made so far, major challenges and ample opportunities co-exist in this field, calling for collaborative efforts by experts from different disciplines. Many photocatalysts, especially those involving molecular photosensitizers, require the use of non-renewable, sacrificial electron donors in CO_2 reduction. A sustainable photocatalytic system should use water as the sole electron donor. In this sense, photoelectrochemical synthesis, which often employ heterogenized molecular CO_2-reduction catalysts on semiconductors with appropriate band structures, appear to be the ultimate solution to address this issue and huge progress has been made in this direction.[163, 164] Innovative design of SACs has allowed effective coupling between CO_2 reduction and water oxidation.[151] The development of photocatalysts based on earth-abundant metals[165] is also important for achieving energy sustainability through solar CO_2 reduction.

In some instances, heterogenization of molecular catalysts could lead to reduced catalytic activity due to detrimental ligand derivatization, in spite of enhanced stability upon surface attachment. This was observed in our studies using Re–bpy and Co–cyclam, as described in Sections 2 and 3. Therefore, effective heterogenization strategies should aim to preserve or even improve the catalytic activity of the metal centers. Research in this area could really benefit from existing knowledge on the effects of ligand derivatization on the activity of molecular catalysts.

It remains a challenge to reveal the exact structures of well-defined surface catalytic sites at the molecular level. Our research demonstrated that combining catalyst synthesis with advanced spectroscopy and theory is a powerful approach to study heterogenized molecular catalysts and SACs. Such an approach could generate critical information beyond just catalyst structures. For example, Lian, Batista, and co-workers[50, 166, 167] employed phase-sensitive sum frequency generation spectroscopy and DFT calculations to interrogate the configuration of Re–bpy on TiO_2 surfaces. The researchers investigated Re–bpy attached to TiO_2 via molecular linkages of various lengths, which could allow effective manipulation of the spatial orientation of Re–bpy on TiO_2 surfaces.

Furthermore, elucidating the unique advantages of heterogenized molecular catalysts and SACs in photocatalysis requires mechanistic studies using ultrafast spectroscopies and in situ/operando techniques.[168-171] As mentioned earlier, results obtained using transient absorption spectroscopy revealed underlying reasons for observed enhancement in the CO_2-reduction activity of Re–bpy upon heterogenization on TiO_2 surfaces.[52, 53] In this sense, one advantage of photocatalysts containing well-defined surface sites lies in the fact that they could utilize techniques from both homogeneous catalysis and heterogenous catalysis.

Acknowledgments

This material is based upon work supported by the U.S. National Science Foundation under awards 1352437 and 2102655, and the U.S. Department of Energy, Office of Science, Office of Basic Energy Sciences under award DE-SC0016417 to G.L. The authors acknowledge collaborations and discussions with Drs. Edward Wong, Richard Johnson, Tijana Rajh, Etsuko Fujita, Dunwei Wang, Anatoly Frenkel, N. Aaron Deskins, Christine A. Caputo, Jonathan Rochford, Gary Brudvig, Victor Batista, Robert Crabtree, and Charles Schmuttenmaer.

References

1. Mikkelsen, M.; Jorgensen, M.; Krebs, F. C., The Teraton Challenge. A Review of Fixation and Transformation of Carbon Dioxide. *Energy Environ. Sci.* **2010,** *3* (1), 43-81.
2. Appel, A. M.; Bercaw, J. E.; Bocarsly, A. B.; Dobbek, H.; DuBois, D. L.; Dupuis, M.; Ferry, J. G.; Fujita, E.; Hille, R.; Kenis, P. J. A.; Kerfeld, C. A.; Morris, R. H.; Peden, C. H. F.; Portis, A. R.; Ragsdale, S. W.; Rauchfuss, T. B.; Reek, J. N. H.; Seefeldt, L. C.; Thauer, R. K.; Waldrop, G. L., Frontiers, Opportunities, and Challenges in Biochemical and Chemical Catalysis of CO_2 Fixation. *Chem. Rev.* **2013,** *113*, 6621-6658.
3. Kumar, B.; Llorente, M.; Froehlich, J.; Dang, T.; Sathrum, A.; Kubiak, C. P., Photochemical and photoelectrochemical reduction of CO_2. *Annu. Rev. Phys. Chem.* **2012,** *63*, 541-569.
4. White, J. L.; Baruch, M. F.; Pander, J. E.; Hu, Y.; Fortmeyer, I. C.; Park, J. E.; Zhang, T.; Liao, K.; Gu, J.; Yan, Y.; Shaw, T. W.; Abelev, E.; Bocarsly, A. B., Light-Driven Heterogeneous Reduction of Carbon Dioxide: Photocatalysts and Photoelectrodes. *Chem. Rev.* **2015,** *115* (23), 12888-12935.
5. Tamaki, Y.; Ishitani, O., Supramolecular Photocatalysts for the Reduction of CO_2. *ACS Catal.* **2017,** *7* (5), 3394-3409.
6. Wang, Y.; He, D.; Chen, H.; Wang, D., Catalysts in electro-, photo- and photoelectrocatalytic CO_2 reduction reactions. *J. Photochem. Photobiol. C: Photochem. Rev.* **2019,** *40*, 117-149.
7. Dalle, K. E.; Warnan, J.; Leung, J. J.; Reuillard, B.; Karmel, I. S.; Reisner, E., Electro- and Solar-Driven Fuel Synthesis with First Row Transition Metal Complexes. *Chem. Rev.* **2019,** *119* (4), 2752-2875.
8. Fujita, E., Photochemical carbon dioxide reduction with metal complexes. *Coord. Chem. Rev.* **1999,** *185-186*, 373-384.
9. Morris, A. J.; Meyer, G. J.; Fujita, E., Molecular Approaches to the Photocatalytic Reduction of Carbon Dioxide for Solar Fuels. *Acc. Chem. Res.* **2009,** *42*, 1983-1994.
10. Windle, C. D.; Perutz, R. N., Advances in molecular photocatalytic and electrocatalytic CO_2 reduction. *Coord. Chem. Rev.* **2012,** *256* (21–22), 2562-2570.

11. Boutin, E.; Merakeb, L.; Ma, B.; Boudy, B.; Wang, M.; Bonin, J.; Anxolabéhère-Mallart, E.; Robert, M., Molecular catalysis of CO_2 reduction: recent advances and perspectives in electrochemical and light-driven processes with selected Fe, Ni and Co aza macrocyclic and polypyridine complexes. *Chem. Soc. Rev.* **2020**, *49*, 5772-5809
12. Hawecker, J.; Lehn, J.-M.; Ziessel, R., Efficient Photochemical Reduction of CO_2 to CO by Visible Light Irradiation of Systems Containing $Re(bipy)(CO)_3X$ or $Ru(bipy)_3^{2+}$-Co^{2+} Combinations as Homogeneous Catalysts. *J. Chem. Soc., Chem. Commun.* **1983**, 536-538.
13. Sahara, G.; Ishitani, O., Efficient Photocatalysts for CO_2 Reduction. *Inorg. Chem.* **2015,** *54* (11), 5096-5104.
14. Fujita, E.; Creutz, C.; Sutin, N.; Szalda, D. J., Carbon dioxide activation by cobalt(I) macrocycles: factors affecting carbon dioxide and carbon monoxide binding. *J. Am. Chem. Soc.* **1991,** *113* (1), 343-353.
15. Matsuoka, S.; Yamamoto, K.; Ogata, T.; Kusaba, M.; Nakashima, N.; Fujita, E.; Yanagida, S., Efficient and selective electron mediation of cobalt complexes with cyclam and related macrocycles in the p-terphenyl-catalyzed photoreduction of carbon dioxide. *J. Am. Chem. Soc.* **1993,** *115* (2), 601-609.
16. Hoffmann, M. R.; Moss, J. A.; Baum, M. M., Artificial photosynthesis: semiconductor photocatalytic fixation of CO_2 to afford higher organic compounds. *Dalton Trans.* **2011,** *40*, 5151-5158.
17. He, H.; Liu, C.; Dubois, K. D.; Jin, T.; Louis, M. E.; Li, G., Enhanced Charge Separation in Nanostructured TiO_2 Materials for Photocatalytic and Photovoltaic Applications. *Ind. Eng. Chem. Res.* **2012,** *51* (37), 11841-11849.
18. Mori, K.; Yamashita, H.; Anpo, M., Photocatalytic reduction of CO_2 with H_2O on various titanium oxide photocatalysts. *RSC Adv.* **2012,** *2*, 3165-3172.
19. Habisreutinger, S. N.; Schmidt-Mende, L.; Stolarczyk, J. K., Photocatalytic Reduction of CO_2 on TiO_2 and Other Semiconductors. *Angew. Chem. Int. Ed.* **2013,** *52*, 7372-7408.
20. Tu, W.; Zhou, Y.; Zou, Z., Photocatalytic Conversion of CO_2 into Renewable Hydrocarbon Fuels: State-of-the-Art Accomplishment, Challenges, and Prospects. *Adv. Mater.* **2014,** *26* (27), 4607-4626.
21. Li, X.; Yu, J.; Jaroniec, M.; Chen, X., Cocatalysts for Selective Photoreduction of CO_2 into Solar Fuels. *Chem. Rev.* **2019,** *119* (6), 3962-4179.
22. Inoue, T.; Fujishima, A.; Konishi, S.; Honda, K., Photoelectrocatalytic reduction of carbon dioxide in aqueous suspensions of semiconductor powders. *Nature* **1979,** *277*, 637-638.
23. Hoffmann, M. R.; Martin, S. T.; Choi, W.; Bahnemann, D. W., Environmental Applications of Semiconductor Photocatalysis. *Chem. Rev.* **1995,** *95* (1), 69-96.
24. Li, G.; Gray, K. A., The solid–solid interface: Explaining the high and unique photocatalytic reactivity of TiO_2-based nanocomposite materials. *Chem. Phys.* **2007,** *339*, 173-187.
25. Tran, P. D.; Wong, L. H.; Barber, J.; Loo, J. S. C., Recent advances in hybrid photocatalysts for solar fuel production. *Energy Environ. Sci.* **2012,** *5*, 5902-5918.
26. Wen, F.; Li, C., Hybrid Artificial Photosynthetic Systems Comprising Semiconductors as Light Harvesters and Biomimetic Complexes as Molecular Cocatalysts. *Acc. Chem. Res.* **2013,** *46* (11), 2355-2364.
27. Windle, C. D.; Reisner, E., Heterogenised Molecular Catalysts for the Reduction of CO_2 to Fuels. *Chimia* **2015,** *69* (7-8), 435-441.

28. Louis, M. E.; Fenton, T. G.; Rondeau, J.; Jin, T.; Li, G., Solar CO_2 Reduction Using Surface-Immobilized Molecular Catalysts. *Comments Inorg. Chem.* **2016,** *36* (1), 38-60.
29. Maeda, K., Metal-Complex/Semiconductor Hybrid Photocatalysts and Photoelectrodes for CO_2 Reduction Driven by Visible Light. *Adv. Mater.* **2019,** *31* (25), 1808205.
30. Perazio, A.; Lowe, G.; Gobetto, R.; Bonin, J.; Robert, M., Light-driven catalytic conversion of CO_2 with heterogenized molecular catalysts based on fourth period transition metals. *Coord. Chem. Rev.* **2021,** *443*, 214018.
31. Reguero, M.; Claver, C.; Carrilho, R. M. B.; Masdeu-Bultó, A. M., Immobilized Molecular Catalysts for CO_2 Photoreduction. *Adv. Sustain. Sys.* **2022,** *6* (6), 2100493.
32. Gates, B. C.; Flytzani-Stephanopoulos, M.; Dixon, D. A.; Katz, A., Atomically dispersed supported metal catalysts: perspectives and suggestions for future research. *Catal. Sci. Technol.* **2017,** *7* (19), 4259-4275.
33. Cui, X.; Li, W.; Ryabchuk, P.; Junge, K.; Beller, M., Bridging homogeneous and heterogeneous catalysis by heterogeneous single-metal-site catalysts. *Nat. Catal.* **2018,** *1* (6), 385-397.
34. Wang, A.; Li, J.; Zhang, T., Heterogeneous single-atom catalysis. *Nat. Rev. Chem.* **2018,** *2* (6), 65-81.
35. Kaiser, S. K.; Chen, Z.; Faust Akl, D.; Mitchell, S.; Pérez-Ramírez, J., Single-Atom Catalysts across the Periodic Table. *Chem. Rev.* **2020,** *120* (21), 11703-11809.
36. Ji, S.; Chen, Y.; Wang, X.; Zhang, Z.; Wang, D.; Li, Y., Chemical Synthesis of Single Atomic Site Catalysts. *Chem. Rev.* **2020,** *120* (21), 11900-11955.
37. Xi, J.; Jung, H. S.; Xu, Y.; Xiao, F.; Bae, J. W.; Wang, S., Synthesis Strategies, Catalytic Applications, and Performance Regulation of Single-Atom Catalysts. *Adv. Funct. Mater.* **2021,** *31* (12), 2008318.
38. Swain, S.; Altaee, A.; Saxena, M.; Samal, A. K., A comprehensive study on heterogeneous single atom catalysis: Current progress, and challenges. *Coord. Chem. Rev.* **2022,** *470*, 214710.
39. Guo, J.; Liu, H.; Li, D.; Wang, J.; Djitcheu, X.; He, D.; Zhang, Q., A minireview on the synthesis of single atom catalysts. *RSC Adv.* **2022,** *12* (15), 9373-9394.
40. Gao, C.; Low, J.; Long, R.; Kong, T.; Zhu, J.; Xiong, Y., Heterogeneous Single-Atom Photocatalysts: Fundamentals and Applications. *Chem. Rev.* **2020,** *120* (21), 12175-12216.
41. Xia, B.; Zhang, Y.; Ran, J.; Jaroniec, M.; Qiao, S.-Z., Single-Atom Photocatalysts for Emerging Reactions. *ACS Cent. Sci.* **2021,** *7* (1), 39-54.
42. Xue, Z.-H.; Luan, D.; Zhang, H.; Lou, X. W., Single-atom catalysts for photocatalytic energy conversion. *Joule* **2022,** *6* (1), 92-133.
43. Zhou, P.; Luo, M.; Guo, S., Optimizing the semiconductor–metal-single-atom interaction for photocatalytic reactivity. *Nat. Rev. Chem.* **2022,** *6* (11), 823-838.
44. Xia, T.; Long, R.; Gao, C.; Xiong, Y., Design of atomically dispersed catalytic sites for photocatalytic CO_2 reduction. *Nanoscale* **2019,** *11* (23), 11064-11070.
45. Zhang, Y.; Xia, B.; Ran, J.; Davey, K.; Qiao, S. Z., Atomic-Level Reactive Sites for Semiconductor-Based Photocatalytic CO_2 Reduction. *Adv. Energy Mater.* **2020,** *10* (9), 1903879.
46. Lu, Y.; Zhang, Z.; Wang, H.; Wang, Y., Toward efficient single-atom catalysts for renewable fuels and chemicals production from biomass and CO_2. *Appl. Catal. B: Environ.* **2021,** *292*, 120162.
47. Hiragond, C. B.; Powar, N. S.; Lee, J.; In, S. I., Single-Atom Catalysts (SACs) for Photocatalytic CO_2 Reduction with H_2O: Activity, Product Selectivity, Stability, and Surface Chemistry. *Small* **2022,** *18* (29), e2201428.

48. Liu, L.; Li, M.; Chen, F.; Huang, H., Recent Advances on Single-Atom Catalysts for CO_2 Reduction. *Small Struct.* **2023,** *4* (3), 2200188.
49. Huang, J.; Stockwell, D.; Huang, Z.; Mohler, D. L.; Lian, T., Photoinduced Ultrafast Electron Transfer from CdSe Quantum Dots to Re-bipyridyl Complexes. *J. Am. Chem. Soc.* **2008,** *130* (17), 5632-5633.
50. Anfuso, C. L.; Snoeberger, R. C., III; Ricks, A. M.; Liu, W.; Xiao, D.; Batista, V. S.; Lian, T., Covalent Attachment of a Rhenium Bipyridyl CO_2 Reduction Catalyst to Rutile TiO_2. *J. Am. Chem. Soc.* **2011,** *133*, 6922-6925.
51. Won, D. I.; Lee, J. S.; Ji, J. M.; Jung, W. J.; Son, H. J.; Pac, C.; Kang, S. O., Highly Robust Hybrid Photocatalyst for Carbon Dioxide Reduction: Tuning and Optimization of Catalytic Activities of Dye/TiO_2/Re(I) Organic-Inorganic Ternary Systems. *J. Am. Chem. Soc.* **2015,** *137* (42), 13679-90.
52. Windle, C. D.; Pastor, E.; Reynal, A.; Whitwood, A. C.; Vaynzof, Y.; Durrant, J. R.; Perutz, R. N.; Reisner, E., Improving the Photocatalytic Reduction of CO_2 to CO through Immobilization of a Molecular Re Catalyst on TiO_2. *Chem. - Eur. J.* **2015,** *21*, 3746-3754.
53. Abdellah, M.; El-Zohry, A. M.; Antila, L. J.; Windle, C. D.; Reisner, E.; Hammarström, L., Time-Resolved IR Spectroscopy Reveals a Mechanism with TiO_2 as a Reversible Electron Acceptor in a TiO_2–Re Catalyst System for CO_2 Photoreduction. *J. Am. Chem. Soc.* **2017,** *139* (3), 1226-1232.
54. Faustino, L. A.; Souza, B. L.; Nunes, B. N.; Duong, A.-T.; Sieland, F.; Bahnemann, D. W.; Patrocinio, A. O. T., Photocatalytic CO_2 Reduction by Re(I) Polypyridyl Complexes Immobilized on Niobates Nanoscrolls. *ACS Sustain. Chem. Eng.* **2018,** *6* (5), 6073-6083.
55. Huang, J.; Gatty, M. G.; Xu, B.; Pati, P. B.; Etman, A. S.; Tian, L.; Sun, J.; Hammarström, L.; Tian, H., Covalently linking $CuInS_2$ quantum dots with a Re catalyst by click reaction for photocatalytic CO_2 reduction. *Dalton Trans.* **2018,** *47* (31), 10775-10783.
56. Orchanian, N. M.; Hong, L. E.; Skrainka, J. A.; Esterhuizen, J. A.; Popov, D. A.; Marinescu, S. C., Surface-Immobilized Conjugated Polymers Incorporating Rhenium Bipyridine Motifs for Electrocatalytic and Photocatalytic CO_2 Reduction. *ACS Appl. Energy Mater.* **2019,** *2* (1), 110-123.
57. Kong, Z.-C.; Zhang, H.-H.; Liao, J.-F.; Dong, Y.-J.; Jiang, Y.; Chen, H.-Y.; Kuang, D.-B., Immobilizing $Re(CO)_3Br(dcbpy)$ Complex on $CsPbBr_3$ Nanocrystal for Boosted Charge Separation and Photocatalytic CO_2 Reduction. *Solar RRL* **2020,** *4* (1), 1900365.
58. Schreier, M.; Luo, J.; Gao, P.; Moehl, T.; Mayer, M. T.; Grätzel, M., Covalent Immobilization of a Molecular Catalyst on Cu_2O Photocathodes for CO_2 Reduction. *J. Am. Chem. Soc.* **2016,** *138* (6), 1938-1946.
59. Kamata, R.; Kumagai, H.; Yamazaki, Y.; Sahara, G.; Ishitani, O., Photoelectrochemical CO_2 Reduction Using a Ru(II)–Re(I) Supramolecular Photocatalyst Connected to a Vinyl Polymer on a NiO Electrode. *ACS Appl. Mater. Interface* **2019,** *11* (6), 5632-5641.
60. Dubois, K. D.; Petushkov, A.; Cardona, E. G.; Larsen, S. C.; Li, G., Adsorption and Photochemical Properties of a Molecular CO_2 Reduction Catalyst in Hierarchical Mesoporous ZSM-5: An In Situ FTIR Study. *J. Phys. Chem. Lett.* **2012,** *3*, 486–492.
61. Dubois, K. D.; He, H.; Liu, C.; Vorushilov, A. S.; Li, G., Covalent attachment of a molecular CO_2-reduction photocatalyst to mesoporous silica. *J. Mol. Catal. A: Chem.* **2012,** *363-364*, 208-213.

62. Liu, C.; Dubois, K. D.; Louis, M. E.; Vorushilov, A. S.; Li, G., Photocatalytic CO_2 Reduction and Surface Immobilization of a Tricarbonyl Re(I) Compound Modified with Amide Groups. *ACS Catal.* **2013,** *3*, 655-662.
63. Takeda, H.; Koike, K.; Morimoto, T.; Inumaru, H.; Ishitani, O., Photochemistry and photocatalysis of rhenium(I) diimine complexes. *Adv. Inorg. Chem.* **2011,** *63*, 137-186.
64. Jia, X.; Nedzbala, H. S.; Bottum, S. R.; Cahoon, J. F.; Concepcion, J. J.; Donley, C. L.; Gang, A.; Han, Q.; Hazari, N.; Kessinger, M. C.; Lockett, M. R.; Mayer, J. M.; Mercado, B. Q.; Meyer, G. J.; Pearce, A. J.; Rooney, C. L.; Sampaio, R. N.; Shang, B.; Wang, H., Synthesis and Surface Attachment of Molecular Re(I) Complexes Supported by Functionalized Bipyridyl Ligands. *Inorg. Chem.* **2023,** *62* (5), 2359-2375.
65. Fenton, T. G.; Louis, M. E.; Li, G., Effect of ligand derivatization at different positions on photochemical properties of hybrid Re(I) photocatalysts. *J. Mol. Catal. A* **2016,** *411*, 272-278.
66. Argazzi, R.; Bignozzi, C. A.; Heimer, T. A.; Castellano, F. N.; Meyer, G. J., Enhanced Spectral Sensitivity from Ruthenium(II) Polypyridyl Based Photovoltaic Devices. *Inorg. Chem.* **1994,** *33* (25), 5741-5749.
67. Guyot, M.; Lalloz, M.-N.; Aguirre-Araque, J. S.; Rogez, G.; Costentin, C.; Chardon-Noblat, S., Rhenium Carbonyl Molecular Catalysts for CO_2 Electroreduction: Effects on Catalysis of Bipyridine Substituents Mimicking Anchorage Functions to Modify Electrodes. *Inorg. Chem.* **2022,** *61* (40), 16072-16080.
68. Ge, A.; Rudshteyn, B.; Videla, P. E.; Miller, C. J.; Kubiak, C. P.; Batista, V. S.; Lian, T., Heterogenized Molecular Catalysts: Vibrational Sum-Frequency Spectroscopic, Electrochemical, and Theoretical Investigations. *Acc. Chem. Res.* **2019,** *52* (5), 1289-1300.
69. Smieja, J. M.; Kubiak, C. P., Re(bipy-tBu)$(CO)_3$Cl-improved Catalytic Activity for Reduction of Carbon Dioxide: IR-Spectroelectrochemical and Mechanistic Studies. *Inorg. Chem.* **2010,** *49* (20), 9283-9289.
70. Morimoto, T.; Nakajima, T.; Sawa, S.; Nakanishi, R.; Imori, D.; Ishitani, O., CO_2 Capture by a Rhenium(I) Complex with the Aid of Triethanolamine. *J. Am. Chem. Soc.* **2013,** *135* (45), 16825-16828.
71. He, H.; Liu, C.; Louis, M. E.; Li, G., Infrared studies of a hybrid CO_2-reduction photocatalyst consisting of a molecular Re(I) complex grafted on Kaolin. *J. Mol. Catal. A* **2014,** *395* (0), 145-150.
72. Maeda, K.; Sekizawa, K.; Ishitani, O., A polymeric-semiconductor-metal-complex hybrid photocatalyst for visible-light CO_2 reduction. *Chem. Commun.* **2013,** *49*, 10127-10129.
73. Neri, G.; Forster, M.; Walsh, J. J.; Robertson, C. M.; Whittles, T. J.; Farras, P.; Cowan, A. J., Photochemical CO_2 reduction in water using a co-immobilised nickel catalyst and a visible light sensitiser. *Chem. Commun.* **2016,** *52* (99), 14200-14203.
74. Rosser, T. E.; Windle, C. D.; Reisner, E., Electrocatalytic and Solar-Driven CO_2 Reduction to CO with a Molecular Manganese Catalyst Immobilized on Mesoporous TiO_2. *Angew. Chem. Int. Ed.* **2016,** *55*, 7388-7392.
75. Kuehnel, M. F.; Sahm, C. D.; Neri, G.; Lee, J. R.; Orchard, Katherine L.; Cowan, A. J.; Reisner, E., ZnSe quantum dots modified with a Ni(cyclam) catalyst for efficient visible-light driven CO_2 reduction in water. *Chem. Sci.* **2018,** *9* (9), 2501-2509.
76. Roy, S.; Reisner, E., Visible-Light-Driven CO_2 Reduction by Mesoporous Carbon Nitride Modified with Polymeric Cobalt Phthalocyanine. *Angew. Chem. Int. Ed.* **2019,** *58* (35), 12180-12184.

77. Ma, B.; Chen, G.; Fave, C.; Chen, L.; Kuriki, R.; Maeda, K.; Ishitani, O.; Lau, T.-C.; Bonin, J.; Robert, M., Efficient Visible-Light-Driven CO_2 Reduction by a Cobalt Molecular Catalyst Covalently Linked to Mesoporous Carbon Nitride. *J. Am. Chem. Soc.* **2020,** *142* (13), 6188-6195.
78. Wang, J.-W.; Gil-Sepulcre, M.; Huang, H.-H.; Solano, E.; Mu, Y.-F.; Llobet, A.; Ouyang, G., CH-π interaction boosts photocatalytic CO_2 reduction activity of a molecular cobalt catalyst anchored on carbon nitride. *Cell Rep. Phys. Sci.* **2021,** *2* (12), 100681.
79. Wei, Y.; Chen, L.; Chen, H.; Cai, L.; Tan, G.; Qiu, Y.; Xiang, Q.; Chen, G.; Lau, T.-C.; Robert, M., Highly Efficient Photocatalytic Reduction of CO_2 to CO by In Situ Formation of a Hybrid Catalytic System Based on Molecular Iron Quaterpyridine Covalently Linked to Carbon Nitride. *Angew. Chem. Int. Ed.* **2022,** *61* (11), e202116832.
80. Sujandi; Prasetyanto, E. A.; Han, D.-S.; Lee, S.-C.; Park, S.-E., Immobilization of Co(III) using tethered cyclam ligand on SBA-15 mesoporous silica for aerial oxidation of ethylbenzene. *Catal. Today* **2009,** *141* (3-4), 374-377.
81. Jin, T.; Liu, C.; Li, G., Heterogenization of a macrocyclic cobalt complex for photocatalytic CO_2 reduction. *J. Coord. Chem.* **2016,** *69* (11-13), 1748-1758.
82. Bosnich, B.; Poon, C. K.; Tobe, M. L., Complexes of cobalt(III) with a cyclic tetradentate secondary amine. *Inorg Chem.* **1965,** *4*, 1102-1108.
83. Froehlich, J. D.; Kubiak, C. P., Homogeneous CO_2 Reduction by Ni(cyclam) at a Glassy Carbon Electrode. *Inorg. Chem.* **2012,** *51* (7), 3932-3934.
84. Forget, A.; Regnacq, M.; Orain, C.; Touzé, E.; Lelong, E.; Brandily, C.; Bernard, H.; Tripier, R.; Le Poul, N., Electrocatalytic reduction of CO_2 in water by a C-functionalized Ni–cyclam complex grafted onto carbon. *Chem. Commun.* **2022,** *58* (48), 6785-6788.
85. Fenton, T.; Gillingham, S.; Jin, T.; Li, G., Microwave-assisted deposition of a highly active cobalt catalyst on mesoporous silica for photochemical CO_2 reduction. *Dalton Trans.* **2017,** *46* (32), 10721-10726.
86. Bosnich, B.; Poon, C. K.; Tobe, M. L., Peroxo complexes of cobalt(III) with a cyclic quadridentate secondary amine. *Inorg. Chem.* **1966,** *5*, 1514-1517.
87. Jin, T.; Liu, C.; Li, G., Photocatalytic CO_2 reduction using a molecular cobalt complex deposited on TiO_2 nanoparticles. *Chem. Commun.* **2014,** *50* (47), 6221-6224.
88. Liu, C.; Jin, T.; Louis, M. E.; Pantovich, S. A.; Skraba-Joiner, S. L.; Rajh, T.; Li, G., Molecular deposition of a macrocyclic cobalt catalyst on TiO_2 nanoparticles. *J. Mol. Catal. A* **2016,** *423*, 293-299.
89. Petsi, T.; Panagiotou, G. D.; Garoufalis, C. S.; Kordulis , C.; Stathi, P.; Deligiannakis, Y.; Lycourghiotis, A.; Bourikas , K., Interfacial Impregnation Chemistry in the Synthesis of Cobalt Catalysts Supported on Titania. *Chem. Eur. J.* **2009,** *15* (47), 13090-13104.
90. Hurum, D. C.; Agrios, A. G.; Gray, K. A.; Rajh, T.; Thurnauer, M. C., Explaining the enhanced photocatalytic activity of Degussa P25 mixed-phase TiO_2 using EPR. *J. Phys. Chem. B* **2003,** *107* (19), 4545-4549.
91. Hurum, D. C.; Gray, K. A.; Rajh, T.; Thurnauer, M. C., Recombination pathways in the Degussa P25 formulation of TiO_2: Surface versus lattice mechanisms. *J. Phys. Chem. B* **2005,** *109* (2), 977-980.
92. Wang, X.; Chen, X.; Thomas, A.; Fu, X.; Antonietti, M., Metal-Containing Carbon Nitride Compounds: A New Functional Organic-Metal Hybrid Material. *Adv. Mater.* **2009,** *21* (16), 1609-1612.

93. Cao, S.; Low, J.; Yu, J.; Jaroniec, M., Polymeric Photocatalysts Based on Graphitic Carbon Nitride. *Adv. Mater.* **2015,** *27* (13), 2150-2176.
94. Ong, W.-J.; Tan, L.-L.; Ng, Y. H.; Yong, S.-T.; Chai, S.-P., Graphitic Carbon Nitride (g-C_3N_4)-Based Photocatalysts for Artificial Photosynthesis and Environmental Remediation: Are We a Step Closer To Achieving Sustainability? *Chem. Rev.* **2016,** *116* (12), 7159-7329.
95. Fang, Y.; Wang, X., Photocatalytic CO_2 conversion by polymeric carbon nitrides. *Chem. Commun.* **2018,** *54* (45), 5674-5687.
96. Liang, J.; Jiang, Z.; Wong, P. K.; Lee, C.-S., Recent Progress on Carbon Nitride and Its Hybrid Photocatalysts for CO_2 Reduction. *Solar RRL* **2021,** *5* (2), 2000478.
97. Liu, R.; Chen, Z.; Yao, Y.; Li, Y.; Cheema, W. A.; Wang, D.; Zhu, S., Recent advancements in g-C_3N_4-based photocatalysts for photocatalytic CO_2 reduction: a mini review. *RSC Adv.* **2020,** *10* (49), 29408-29418.
98. Kuriki, R.; Matsunaga, H.; Nakashima, T.; Wada, K.; Yamakata, A.; Ishitani, O.; Maeda, K., Nature-Inspired, Highly Durable CO_2 Reduction System Consisting of a Binuclear Ruthenium(II) Complex and an Organic Semiconductor Using Visible Light. *J. Am. Chem. Soc.* **2016,** *138* (15), 5159-5170.
99. Cometto, C.; Kuriki, R.; Chen, L.; Maeda, K.; Lau, T.-C.; Ishitani, O.; Robert, M., A Carbon Nitride/Fe Quaterpyridine Catalytic System for Photostimulated CO_2-to-CO Conversion with Visible Light. *J. Am. Chem. Soc.* **2018,** *140* (24), 7437-7440.
100. Zheng, J.; Li, X.; Qin, Y.; Zhang, S.; Sun, M.; Duan, X.; Sun, H.; Li, P.; Wang, S., Zn phthalocyanine/carbon nitride heterojunction for visible light photoelectrocatalytic conversion of CO_2 to methanol. *J. Catal.* **2019,** *371*, 214-223.
101. Huang, P.; Pantovich, S. A.; Okolie, N. O.; Deskins, N. A.; Li, G., Hybrid Carbon Dioxide Reduction Photocatalysts Consisting of Macrocyclic Cobalt(III) Complexes Deposited on Semiconductor Surfaces. *ChemPhotoChem* **2020,** *4* (6), 420-426.
102. Pan, Z.; Niu, P.; Liu, M.; Zhang, G.; Zhu, Z.; Wang, X., Molecular Junctions on Polymeric Carbon Nitrides with Enhanced Photocatalytic Performance. *ChemSusChem* **2020,** *13* (5), 888-892.
103. Zhen, W.; Xue, C., Atomic- and Molecular-Level Functionalizations of Polymeric Carbon Nitride for Solar Fuel Production. *Solar RRL* **2021,** *5* (2), 2000440.
104. Shang, B.; Zhao, F.; Choi, C.; Jia, X.; Pauly, M.; Wu, Y.; Tao, Z.; Zhong, Y.; Harmon, N.; Maggard, P. A.; Lian, T.; Hazari, N.; Wang, H., Monolayer Molecular Functionalization Enabled by Acid–Base Interaction for High-Performance Photochemical CO_2 Reduction. *ACS Energy Lett.* **2022,** *7* (7), 2265-2272.
105. Li, J.; Huang, P.; Guo, F.; Huang, J.; Xiang, S.; Yang, K.; Deskins, N. A.; Batista, V. S.; Li, G.; Frenkel, A. I., X-ray Absorption Spectroscopy Studies of a Molecular CO_2-Reduction Catalyst Deposited on Graphitic Carbon Nitride. *J. Phys. Chem. C* **2023,** *127* (7), 3626-3633.
106. Xiang, S.; Huang, P.; Li, J.; Liu, Y.; Marcella, N.; Routh, P. K.; Li, G.; Frenkel, A. I., Solving the structure of "single-atom" catalysts using machine learning – assisted XANES analysis. *Phys. Chem. Chem. Phys.* **2022,** *24* (8), 5116-5124.
107. Timoshenko, J.; Duan, Z.; Henkelman, G.; Crooks, R. M.; Frenkel, A. I., Solving the Structure and Dynamics of Metal Nanoparticles by Combining X-Ray Absorption Fine Structure Spectroscopy and Atomistic Structure Simulations. *Annu. Rev. Anal. Chem.* **2019,** *12* (1), 501-522.
108. Ankudinov, A. L.; Ravel, B.; Rehr, J. J.; Conradson, S. D., Real-space multiple-scattering calculation and interpretation of x-ray-absorption near-edge structure. *Phys. Rev. B* **1998,** *58* (12), 7565-7576.

109. Fujita, E.; Furenlid, L. R.; Renner, M. W., Direct XANES Evidence for Charge Transfer in Co-CO_2 Complexes. *J. Am. Chem. Soc.* **1997,** *119* (19), 4549-4550.
110. Zhang, T.; Lin, W., Metal-organic frameworks for artificial photosynthesis and photocatalysis. *Chem. Soc. Rev.* **2014,** *43* (16), 5982-5993.
111. Wang, C.-C.; Zhang, Y.-Q.; Li, J.; Wang, P., Photocatalytic CO_2 reduction in metal-organic frameworks: A mini review. *J. Mol. Struct.* **2015,** *1083*, 127-136.
112. Wang, Q.; Zhang, Y.; Lin, H.; Zhu, J., Recent Advances in Metal-Organic Frameworks for Photo-/Electrocatalytic CO_2 Reduction. *Chem. - Eur. J.* **2019,** *25* (62), 14026-14035.
113. Takeda, H.; Ohashi, M.; Tani, T.; Ishitani, O.; Inagaki, S., Enhanced Photocatalysis of Rhenium(I) Complex by Light-Harvesting Periodic Mesoporous Organosilica. *Inorg. Chem.* **2010,** *49* (10), 4554-4559.
114. Wang, C.; Xie, Z.; deKrafft, K. E.; Lin, W., Doping Metal-Organic Frameworks for Water Oxidation, Carbon Dioxide Reduction, and Organic Photocatalysis. *J. Am. Chem. Soc.* **2011,** *133* (34), 13445–13454.
115. Yang, S.; Hu, W.; Zhang, X.; He, P.; Pattengale, B.; Liu, C.; Cendejas, M.; Hermans, I.; Zhang, X.; Zhang, J.; Huang, J., 2D Covalent Organic Frameworks as Intrinsic Photocatalysts for Visible Light-Driven CO_2 Reduction. *J. Am. Chem. Soc.* **2018,** *140* (44), 14614-14618.
116. Zhu, J.; Usov, P. M.; Xu, W.; Celis-Salazar, P. J.; Lin, S.; Kessinger, M. C.; Landaverde-Alvarado, C.; Cai, M.; May, A. M.; Slebodnick, C.; Zhu, D.; Senanayake, S. D.; Morris, A. J., A New Class of Metal-Cyclam-Based Zirconium Metal–Organic Frameworks for CO_2 Adsorption and Chemical Fixation. *J. Am. Chem. Soc.* **2018,** *140* (3), 993-1003.
117. Nakamura, R.; Okamoto, A.; Osawa, H.; Irie, H.; Hashimoto, K., Design of All-Inorganic Molecular-Based Photocatalysts Sensitive to Visible Light: Ti(IV)-O-Ce(III) Bimetallic Assemblies on Mesoporous Silica. *J. Am. Chem. Soc.* **2007,** *129* (31), 9596-9597.
118. Kim, W.; Yuan, G.; McClure, B. A.; Frei, H., Light Induced Carbon Dioxide Reduction by Water at Binuclear $ZrOCo^{II}$ Unit Coupled to Ir Oxide Nanocluster Catalyst. *J. Am. Chem. Soc.* **2014,** *136* (31), 11034-11042.
119. Kim, W.; Edri, E.; Frei, H., Hierarchical Inorganic Assemblies for Artificial Photosynthesis. *Acc. Chem. Res.* **2016,** *49*, 1634-1645.
120. Zhong, W.; Sa, R.; Li, L.; He, Y.; Li, L.; Bi, J.; Zhuang, Z.; Yu, Y.; Zou, Z., A Covalent Organic Framework Bearing Single Ni Sites as a Synergistic Photocatalyst for Selective Photoreduction of CO_2 to CO. *J. Am. Chem. Soc.* **2019,** *141* (18), 7615-7621.
121. Wei, Y.-S.; Zhang, M.; Zou, R.; Xu, Q., Metal–Organic Framework-Based Catalysts with Single Metal Sites. *Chem. Rev.* **2020,** *120* (21), 12089-12174.
122. Hou, C.-C.; Wang, H.-F.; Li, C.; Xu, Q., From metal-organic frameworks to single/dual-atom and cluster metal catalysts for energy applications. *Energy Environ. Sci.* **2020,** *13* (6), 1658-1693.
123. Ran, L.; Li, Z.; Ran, B.; Cao, J.; Zhao, Y.; Shao, T.; Song, Y.; Leung, M. K. H.; Sun, L.; Hou, J., Engineering Single-Atom Active Sites on Covalent Organic Frameworks for Boosting CO_2 Photoreduction. *J. Am. Chem. Soc.* **2022,** *144* (37), 17097-17109.
124. Wagner, A.; Sahm, C. D.; Reisner, E., Towards molecular understanding of local chemical environment effects in electro- and photocatalytic CO_2 reduction. *Nat. Catal.* **2020,** *3* (10), 775-786.
125. Li, X.; Liu, L.; Ren, X.; Gao, J.; Huang, Y.; Liu, B., Microenvironment modulation of single-atom catalysts and their roles in electrochemical energy conversion. *Sci. Adv.* **2020,** *6* (39), eabb6833.

126. Soucy, T. L.; Dean, W. S.; Zhou, J.; Rivera Cruz, K. E.; McCrory, C. C. L., Considering the Influence of Polymer–Catalyst Interactions on the Chemical Microenvironment of Electrocatalysts for the CO_2 Reduction Reaction. *Acc. Chem. Res.* **2022,** *55* (3), 252-261.
127. Pan, Y.; Lin, R.; Chen, Y.; Liu, S.; Zhu, W.; Cao, X.; Chen, W.; Wu, K.; Cheong, W.-C.; Wang, Y.; Zheng, L.; Luo, J.; Lin, Y.; Liu, Y.; Liu, C.; Li, J.; Lu, Q.; Chen, X.; Wang, D.; Peng, Q.; Chen, C.; Li, Y., Design of Single-Atom Co–N5 Catalytic Site: A Robust Electrocatalyst for CO_2 Reduction with Nearly 100% CO Selectivity and Remarkable Stability. *J. Am. Chem. Soc.* **2018,** *140* (12), 4218-4221.
128. Mohd Adli, N.; Shan, W.; Hwang, S.; Samarakoon, W.; Karakalos, S.; Li, Y.; Cullen, D. A.; Su, D.; Feng, Z.; Wang, G.; Wu, G., Engineering Atomically Dispersed FeN_4 Active Sites for CO_2 Electroreduction. *Angew. Chem. Int. Ed.* **2021,** *60* (2), 1022-1032.
129. Pan, F.; Zhang, H.; Liu, K.; Cullen, D.; More, K.; Wang, M.; Feng, Z.; Wang, G.; Wu, G.; Li, Y., Unveiling Active Sites of CO_2 Reduction on Nitrogen-Coordinated and Atomically Dispersed Iron and Cobalt Catalysts. *ACS Catal.* **2018,** *8* (4), 3116-3122.
130. Wang, Y.; Mao, J.; Meng, X.; Yu, L.; Deng, D.; Bao, X., Catalysis with Two-Dimensional Materials Confining Single Atoms: Concept, Design, and Applications. *Chem. Rev.* **2019,** *119* (3), 1806-1854.
131. Qin, D.; Zhou, Y.; Wang, W.; Zhang, C.; Zeng, G.; Huang, D.; Wang, L.; Wang, H.; Yang, Y.; Lei, L.; Chen, S.; He, D., Recent advances in two-dimensional nanomaterials for photocatalytic reduction of CO_2: insights into performance, theories and perspective. *J. Mater. Chem. A* **2020,** *8* (37), 19156-19195.
132. Lin, X.; Ng, S.-F.; Ong, W.-J., Coordinating single-atom catalysts on two-dimensional nanomaterials: A paradigm towards bolstered photocatalytic energy conversion. *Coord. Chem. Rev.* **2022,** *471*, 214743.
133. Li, Y.; Kong, T.; Shen, S., Artificial Photosynthesis with Polymeric Carbon Nitride: When Meeting Metal Nanoparticles, Single Atoms, and Molecular Complexes. *Small* **2019,** *15* (32), 1900772.
134. Fu, J.; Wang, S.; Wang, Z.; Liu, K.; Li, H.; Liu, H.; Hu, J.; Xu, X.; Li, H.; Liu, M., Graphitic carbon nitride based single-atom photocatalysts. *Front. Phys.* **2020,** *15* (3), 33201.
135. Zhao, M.; Feng, J.; Yang, W.; Song, S.; Zhang, H., Recent Advances in Graphitic Carbon Nitride Supported Single-Atom Catalysts for Energy Conversion. *ChemCatChem* **2021,** *13* (5), 1250-1270.
136. Huang, P.; Huang, J.; Pantovich, S. A.; Carl, A. D.; Fenton, T. G.; Caputo, C. A.; Grimm, R. L.; Frenkel, A. I.; Li, G., Selective CO_2 Reduction Catalyzed by Single Cobalt Sites on Carbon Nitride under Visible-Light Irradiation. *J. Am. Chem. Soc.* **2018,** *140* (47), 16042-16047.
137. Wang, J.; Heil, T.; Zhu, B.; Tung, C.-W.; Yu, J.; Chen, H. M.; Antonietti, M.; Cao, S., A Single Cu-Center Containing Enzyme-Mimic Enabling Full Photosynthesis under CO_2 Reduction. *ACS Nano* **2020,** *14* (7), 8584-8593.
138. Yang, Y.; Li, F.; Chen, J.; Fan, J.; Xiang, Q., Single Au Atoms Anchored on Amino-Group-Enriched Graphitic Carbon Nitride for Photocatalytic CO_2 Reduction. *ChemSusChem* **2020,** *13* (8), 1979-1985.
139. Li, Y.; Li, B.; Zhang, D.; Cheng, L.; Xiang, Q., Crystalline Carbon Nitride Supported Copper Single Atoms for Photocatalytic CO_2 Reduction with Nearly 100% CO Selectivity. *ACS Nano* **2020,** *14* (8), 10552-10561.

140. Chen, P.; Lei, B.; Dong, X. a.; Wang, H.; Sheng, J.; Cui, W.; Li, J.; Sun, Y.; Wang, Z.; Dong, F., Rare-Earth Single-Atom La–N Charge-Transfer Bridge on Carbon Nitride for Highly Efficient and Selective Photocatalytic CO_2 Reduction. *ACS Nano* **2020,** *14* (11), 15841-15852.
141. Ji, S.; Qu, Y.; Wang, T.; Chen, Y.; Wang, G.; Li, X.; Dong, J.; Chen, Q.; Zhang, W.; Zhang, Z.; Liang, S.; Yu, R.; Wang, Y.; Wang, D.; Li, Y., Rare-Earth Single Erbium Atoms for Enhanced Photocatalytic CO_2 Reduction. *Angew. Chem. Int. Ed.* **2020,** *59* (26), 10651-10657.
142. Cheng, L.; Yin, H.; Cai, C.; Fan, J.; Xiang, Q., Single Ni Atoms Anchored on Porous Few-Layer g-C_3N_4 for Photocatalytic CO_2 Reduction: The Role of Edge Confinement. *Small* **2020,** *16* (28), 2002411.
143. Fu, J.; Zhu, L.; Jiang, K.; Liu, K.; Wang, Z.; Qiu, X.; Li, H.; Hu, J.; Pan, H.; Lu, Y.-R.; Chan, T.-S.; Liu, M., Activation of CO_2 on graphitic carbon nitride supported single-atom cobalt sites. *Chem. Eng. J.* **2021,** *415*, 128982.
144. Cometto, C.; Ugolotti, A.; Grazietti, E.; Moretto, A.; Bottaro, G.; Armelao, L.; Di Valentin, C.; Calvillo, L.; Granozzi, G., Copper single-atoms embedded in 2D graphitic carbon nitride for the CO_2 reduction. *npj 2D Mater. Appl.* **2021,** *5* (1), 63.
145. Zhao, Z.; Liu, W.; Shi, Y.; Zhang, H.; Song, X.; Shang, W.; Hao, C., An insight into the reaction mechanism of CO_2 photoreduction catalyzed by atomically dispersed Fe atoms supported on graphitic carbon nitride. *Phys. Chem. Chem. Phys.* **2021,** *23* (8), 4690-4699.
146. Zhang, J.-H.; Yang, W.; Zhang, M.; Wang, H.-J.; Si, R.; Zhong, D.-C.; Lu, T.-B., Metal-organic layers as a platform for developing single-atom catalysts for photochemical CO_2 reduction. *Nano Energy* **2021,** *80*, 105542.
147. Sharma, P.; Kumar, S.; Tomanec, O.; Petr, M.; Zhu Chen, J.; Miller, J. T.; Varma, R. S.; Gawande, M. B.; Zbořil, R., Carbon Nitride-Based Ruthenium Single Atom Photocatalyst for CO_2 Reduction to Methanol. *Small* **2021,** *17* (16), 2006478.
148. Pollak, N.; Huang, P.; Bell, H.; Li, G.; Caputo, C. A., Tunable Photocatalytic Production of Syngas Using Co@C_3N_4 and Black Phosphorus. *ChemPhotoChem* **2021,** *5* (7), 674-679.
149. Wang, Y.; Qu, Y.; Qu, B.; Bai, L.; Liu, Y.; Yang, Z.-D.; Zhang, W.; Jing, L.; Fu, H., Construction of Six-Oxygen-Coordinated Single Ni Sites on g-C_3N_4 with Boron-Oxo Species for Photocatalytic Water-Activation-Induced CO_2 Reduction. *Adv. Mater.* **2021,** *33* (48), 2105482.
150. Sun, X.; Sun, L.; Li, G.; Tuo, Y.; Ye, C.; Yang, J.; Low, J.; Yu, X.; Bitter, J. H.; Lei, Y.; Wang, D.; Li, Y., Phosphorus Tailors the d-Band Center of Copper Atomic Sites for Efficient CO_2 Photoreduction under Visible-Light Irradiation. *Angew. Chem. Int. Ed.* **2022,** *61* (38), e202207677.
151. Ou, H.; Ning, S.; Zhu, P.; Chen, S.; Han, A.; Kang, Q.; Hu, Z.; Ye, J.; Wang, D.; Li, Y., Carbon Nitride Photocatalysts with Integrated Oxidation and Reduction Atomic Active Centers for Improved CO_2 Conversion. *Angew. Chem. Int. Ed.* **2022,** *61* (34), e202206579.
152. Gao, G.; Jiao, Y.; Waclawik, E. R.; Du, A., Single Atom (Pd/Pt) Supported on Graphitic Carbon Nitride as an Efficient Photocatalyst for Visible-Light Reduction of Carbon Dioxide. *J. Am. Chem. Soc.* **2016,** *138* (19), 6292-6297.
153. Xiao, X.; Gao, Y.; Zhang, L.; Zhang, J.; Zhang, Q.; Li, Q.; Bao, H.; Zhou, J.; Miao, S.; Chen, N.; Wang, J.; Jiang, B.; Tian, C.; Fu, H., A Promoted Charge Separation/Transfer System from Cu Single Atoms and C_3N_4 Layers for Efficient Photocatalysis. *Adv. Mater.* **2020,** *32* (33), 2003082.
154. Cao, Y.; Chen, S.; Luo, Q.; Yan, H.; Lin, Y.; Liu, W.; Cao, L.; Lu, J.; Yang, J.; Yao, T.; Wei, S., Atomic-Level Insight into Optimizing the Hydrogen Evolution Pathway over a Co1-N4 Single-Site Photocatalyst. *Angew. Chem. Int. Ed.* **2017,** *56* (40), 12191-12196.

155. Chen, Z.; Mitchell, S.; Vorobyeva, E.; Leary, R. K.; Hauert, R.; Furnival, T.; Ramasse, Q. M.; Thomas, J. M.; Midgley, P. A.; Dontsova, D.; Antonietti, M.; Pogodin, S.; López, N.; Pérez-Ramírez, J., Stabilization of Single Metal Atoms on Graphitic Carbon Nitride. *Adv. Funct. Mater.* **2017,** *27* (8), 1605785.
156. Yu, F.; Huo, T.; Deng, Q.; Wang, G.; Xia, Y.; Li, H.; Hou, W., Single-atom cobalt-hydroxyl modification of polymeric carbon nitride for highly enhanced photocatalytic water oxidation: ball milling increased single atom loading. *Chem. Sci.* **2022,** *13* (3), 754-762.
157. Huang, P.; Huang, J.; Li, J.; Pham, T. D.; Zhang, L.; He, J.; Brudvig, G. W.; Deskins, N. A.; Frenkel, A. I.; Li, G., Revealing the Structure of Single Cobalt Sites in Carbon Nitride for Photocatalytic CO_2 Reduction. *J. Phys. Chem. C* **2022,** *126* (20), 8596-8604.
158. Li, J.; Zhang, H.; Samarakoon, W.; Shan, W.; Cullen, D. A.; Karakalos, S.; Chen, M.; Gu, D.; More, K. L.; Wang, G.; Feng, Z.; Wang, Z.; Wu, G., Thermally Driven Structure and Performance Evolution of Atomically Dispersed FeN_4 Sites for Oxygen Reduction. *Angew. Chem. Int. Ed.* **2019,** *58* (52), 18971-18980.
159. Qin, X.; Zhu, S.; Xiao, F.; Zhang, L.; Shao, M., Active Sites on Heterogeneous Single-Iron-Atom Electrocatalysts in CO_2 Reduction Reaction. *ACS Energy Lett.* **2019,** *4* (7), 1778-1783.
160. Huang, P.; Huang, J.; Li, J.; Zhang, L.; He, J.; Caputo, C. A.; Frenkel, A. I.; Li, G., Effect of Carbon Doping on CO_2-Reduction Activity of Single Cobalt Sites in Graphitic Carbon Nitride. *ChemNanoMat* **2021,** *7* (9), 1051-1056.
161. Jiang, L.; Yuan, X.; Pan, Y.; Liang, J.; Zeng, G.; Wu, Z.; Wang, H., Doping of graphitic carbon nitride for photocatalysis: A reveiw. *Appl. Catal. B: Environ.* **2017,** *217*, 388-406.
162. Vijay, S.; Ju, W.; Brückner, S.; Tsang, S.-C.; Strasser, P.; Chan, K., Unified mechanistic understanding of CO_2 reduction to CO on transition metal and single atom catalysts. *Nat. Catal.* **2021**.
163. Sato, S.; Arai, T.; Morikawa, T., Toward Solar-Driven Photocatalytic CO_2 Reduction Using Water as an Electron Donor. *Inorg. Chem.* **2015,** *54* (11), 5105-5113.
164. Kumaravel, V.; Bartlett, J.; Pillai, S. C., Photoelectrochemical Conversion of Carbon Dioxide (CO_2) into Fuels and Value-Added Products. *ACS Energy Lett.* **2020,** *5* (2), 486-519.
165. Takeda, H.; Cometto, C.; Ishitani, O.; Robert, M., Electrons, Photons, Protons and Earth-Abundant Metal Complexes for Molecular Catalysis of CO_2 Reduction. *ACS Catal.* **2017,** *7* (1), 70-88.
166. Anfuso, C. L.; Xiao, D.; Ricks, A. M.; Negre, C. F. A.; Batista, V. S.; Lian, T., Orientation of a Series of CO_2 Reduction Catalysts on Single Crystal TiO_2 Probed by Phase-Sensitive Vibrational Sum Frequency Generation Spectroscopy (PS-VSFG). *J. Phys. Chem. C* **2012,** *116*, 24107-24114.
167. Ge, A.; Rudshteyn, B.; Psciuk, B. T.; Xiao, D.; Song, J.; Anfuso, C. L.; Ricks, A. M.; Batista, V. S.; Lian, T., Surface-Induced Anisotropic Binding of a Rhenium CO_2-Reduction Catalyst on Rutile TiO_2(110) Surfaces. *J. Phys. Chem. C* **2016,** *120*, 20970-20977.
168. Li, X.; Yang, X.; Zhang, J.; Huang, Y.; Liu, B., In Situ/Operando Techniques for Characterization of Single-Atom Catalysts. *ACS Catal.* **2019,** *9* (3), 2521-2531.
169. Li, X.; Wang, S.; Li, L.; Sun, Y.; Xie, Y., Progress and Perspective for In Situ Studies of CO_2 Reduction. *J. Am. Chem. Soc.* **2020**, *142*, 9567–9581.
170. Zhang, T.; Chen, Z.; Walsh, A. G.; Li, Y.; Zhang, P., Single-Atom Catalysts Supported by Crystalline Porous Materials: Views from the Inside. *Adv. Mater.* **2020,** *32* (44), 2002910.
171. Hasa, B.; Zhao, Y.; Jiao, F., In Situ/Operando Characterization Techniques of Electrochemical CO_2 Reduction. *Annu. Rev. Chem. Biomol. Eng.* **2023,** *14* (1), 165-185.